

NASA Contractor Report 3341

NASA  
CR  
3341  
c. 1

LOAN COPY  
AFWL TECHNICAL  
KILLAND AFB

0061945



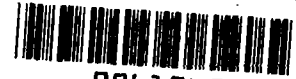
TECH LIBRARY KAFB, NM

Single-Mode Laser Studies:  
(I) Design and Performance of a  
Fixed-Wavelength Laser Source and  
(II) Coupling of Lasers to  
Thin-Film Optical Waveguides

I. Ladany and J. M. Hammer

CONTRACT NAS1-15440  
OCTOBER 1980

**NASA**



NASA Contractor Report 3341

Single-Mode Laser Studies:  
(I) Design and Performance of a  
Fixed-Wavelength Laser Source and  
(II) Coupling of Lasers to  
Thin-Film Optical Waveguides

I. Ladany and J. M. Hammer  
*RCA Laboratories*  
*Princeton, New Jersey*

Prepared for  
Langley Research Center  
under Contract NAS1-15440



National Aeronautics  
and Space Administration

Scientific and Technical  
Information Branch

1980



## PREFACE

This final report covers work done at RCA Laboratories during the period July 3, 1979 to April 3, 1980 under contract No. NAS1-15440. This work was performed in the Solid State Devices Laboratory, under the direction of B. Hershenov. The Group Head was M. E. Ettenberg and the Project Scientist was I. Ladany. Part I of this report was written by I. Ladany and Part II by J. M. Hammer. Staff members and support personnel who contributed to this work in addition to the authors, and the area of their contribution, are listed below:

- D. Botez\* - Single-mode lasers
- L. Elbaum - Fiber coupling
- D. Gilbert - Spectral measurements, temperature-dependence studies
- M. Harvey - Device fabrication
- C. C. Neal - Coupling measurements, lens and prism mount design
- J. O. Schroeder\* - Design and construction of temperature-control circuits

---

\*Members of Technical Staff.



## TABLE OF CONTENTS

Section	Page
INTRODUCTION .....	1
I. DESIGN AND PERFORMANCE OF A FIXED-WAVELENGTH LASER SOURCE MODULE .....	3
A. Objective .....	3
B. Module Design .....	4
1. Temperature Control Circuit .....	4
2. Laser Driver .....	8
C. Theoretical Discussion .....	8
D. Experimental Results .....	12
1. Temperature-Induced Wavelength Changes .....	12
2. Output Fluctuations Due to Temperature Cycling.	17
3. Optical Feedback Effects .....	20
II. COUPLING OF SINGLE-MODE LASERS TO THIN-FILM OPTICAL WAVEGUIDES .....	23
A. Introduction .....	23
B. Selective Grating Coupling .....	25
C. Miniature Cylindrical Lens System for Collecting, Symmetrizing, and Focusing Junction Laser Beams ...	32
1. Introduction .....	32
2. Theory .....	33
D. Prism Coupling to Optical Waveguides .....	40
E. Experimental Observations and Device Construction .	43
III. CONCLUSIONS .....	52
REFERENCES .....	54

## LIST OF ILLUSTRATIONS

Figure	Page
1. Details of the CDH structure .....	2
2. Photograph of the PC board showing parts layout .....	5
3. Temperature control circuit .....	6
4. (a) Photograph of interior of complete unit .....	7
(b) Exterior of complete unit .....	7
5. Driver IC functional diagram .....	9
6. Wavelength shift vs temperature .....	14
7. Wavelength dependence on duty cycle, CDH laser .....	15
8. Output spikes due to TE pulsing .....	17
9. Comparison of fiber output with temperature of the MCB. (a) Laser driven with separate power supply, (b) laser driven with internal IC, and (c) temperature of MCB ....	18
10. Laser output (measured at fiber end) for 19 and 25°C ...	19
11. Optical feedback effects: (a) is output from laser before coupling; (b) after coupling to graded index fiber having the input end beaded as in photomicrograph; (c) same as (b) except that the end of the fiber (away from laser) was immersed in high index fluid; (d) output from fiber with more rounded input end .....	21
12. Thin-film waveguide and corrugated grating coupler. The amplitude of the grating is exaggerated .....	26
13. Selectivity of waveguide grating coupler. The grating space and angle are chosen to optimize the coupling at $\lambda_0$ . $I_0$ is the intensity coupled at $\lambda_0$ . $I$ the intensity coupled at some other wavelength $\lambda$ .....	28

LIST OF ILLUSTRATIONS (Continued)

Figure	Page
14. Traces of the spectral output. Lower trace: directly from the junction laser; upper trace: light grating coupling into LNT waveguide and prism coupled out of waveguide .....	31
15. Perspective illustration of cylinder lens system for symmetrizing junction laser output .....	33
16. Ray diagram for calculating cylinder lens parameters to symmetrize junction laser output. The lateral direction is shown by dashed lines and has been rotated 90° around the Z axis .....	34
17. Plot of $D_L/D_T$ and $A_L/D_T$ as a function of normalized beam waist $W/\lambda_0$ . The lens output "convergence" angle $\theta_1$ is shown on the upper scale. The refractive index of the transverse lens $n_T$ is the parameter .....	39
18. Plot of $G/D_T$ and $\theta/\theta_M$ vs $W/\lambda_0$ ; $n_T$ is the parameter. When $G < 0$ , the lenses overlap. When $\theta/\theta_n > 1$ , not all of the laser light is collected at $n = 1.8$ $G/D_T < 0$ (negative) when $W/\lambda_0 \sim 2.0$ .....	40
19. Schematic diagram of a waveguide-prism film coupler ....	41
20. Sketch of an improved cylinder lens holder. The slots are spaced so that the gap is zero. Shims are used to give the desired gap and the cylinders are cemented into place .....	44
21. Experimental x-y trace of the lateral and transverse beam waist. The center figure is on x-y tracing of the far-field pattern of light coupled out of the LNT guide .....	45
22. Schematic of laser-cylinder lens LNT waveguide assembly.	46



LIST OF ILLUSTRATIONS (Continued)

Figure	Page
23. Cross-section of mechanical module showing details of laser-lens-LNT waveguide mount .....	46
24. Photograph of final laser-lens-waveguide module .....	48
25. Photograph of laser-lens-waveguide module in protective plastic case .....	49
26. Plot of laser power vs laser drive current and spectrum of laser output .....	50
27. Plot of light intensity output of lens system vs laser drive current and spectrum of lens system output. The input is that shown in Fig. 26 .....	50
28. Plot of light intensity output coupled out of LNT guide of module vs laser current and spectrum of same. The input is that shown in Fig. 27 .....	51

## INTRODUCTION

Various schemes have been developed in recent years for obtaining single-mode injection lasers. The most practical devices of this type seem to be those in which lateral mode confinement is built into the laser structure. RCA's version of this device, called the CDH (Constricted Double Heterostructure) laser, is illustrated in Fig. 1. The lateral confinement is obtained by introducing a variation in the cavity thickness, which leads to an index of refraction variation in the plane of the junction. This index variation forms a fixed waveguide which, when properly designed, supports only a fundamental lateral mode. The transverse mode which lies in the plane perpendicular to the junction plane is also supported by a fixed waveguide and is constrained to be fundamental by the index changes at the (AlGa)As heterojunctions and the thickness of the active region. The longitudinal or spectral mode is fixed by the cleaved mirror spacing and there is no built-in selection as there is for the spatial modes (transverse and lateral). For the CDH laser, in common with other lasers of this index-guided type, if the Fabry-Perot cavity is kept short and the material quality high, one longitudinal mode dominates over a considerable current range. In this sense, such a laser is called a single-mode laser.

There have not been too many practical applications for single-mode lasers described in the literature. For highest data rates and longest fiber links such lasers are expected to be of importance, but there are other interesting applications where single-mode lasers will also prove useful.

In the present report we discuss one such application, the utilization of single-mode lasers as fixed-wavelength sources to be used to provide wavelength multiplexing capability in optical-fiber data links. In order to gain full benefit from the use of such lasers it

is necessary to couple their radiation into suitable structures. The second part of this report covers a study of the coupling of single-mode lasers into thin-film optical waveguides.

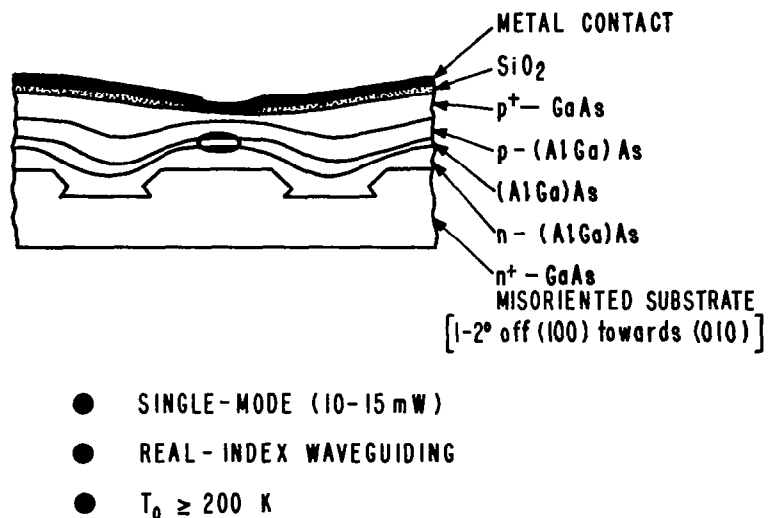


Figure 1. Details of the CDH structure.

Use of trade names or names of manufacturers in this report does not constitute an official endorsement of such products or manufacturers, either expressed or implied, by the National Aeronautics and Space Administration.

# I. DESIGN AND PERFORMANCE OF A FIXED-WAVELENGTH LASER SOURCE MODULE

## A. OBJECTIVE

The objective of the first part of this program was to design and build temperature-stabilized modules for driving RCA-developed single-mode lasers. In use, four separate modules drive four lasers operating at different wavelengths at least 75 Å apart, the lasers being permanently coupled to short lengths of multimode graded-index fibers. These modules are intended for a wavelength multiplexing experiment under development by NASA and its contractors. While modules to drive and stabilize the power output of lasers have been designed previously, there has been no previous attempt to prove a working device which stabilizes the spectral output of a laser.

Detailed specifications for the module are listed in Table 1.

TABLE 1. MODULE SPECIFICATIONS

<u>Parameter</u>	<u>Value</u>
Overall Size	7.6x7.6 cm or smaller
Driver	Fiber-optic transmitter type 2144
Power Supply	+ 5 Vdc
Wavelengths	Four separate values, at least 75 Å apart, with 10-Å stability against temperature changes.
Power	At least 1.5 mW into fiber
Fiber	ITT graded-index, type 201
Maximum Laser Current	150 mA

## B. MODULE DESIGN

The design of the driver module was largely dictated by various NASA requirements. The overall size was set by the need to incorporate a cable connector on one side and a fiber-optic bulkhead connector on the other. Furthermore, it was necessary to provide a convenient storage method for a 30- to 40-cm length of fiber. It was decided to place all the circuits on one board, as shown in Fig. 2. The thermoelectric element (TE) is mounted through the middle of the board, directly to the baseplate. Special identification of some terminals has been made, as they are used in setting the laser current.

### 1. Temperature Control Circuit

In order to maintain the size and voltage specifications, a transformerless circuit was designed to control the current through the TE, and thus the laser temperature. A diagram of this circuit is shown in Fig. 3. Temperature is sensed by a thermistor mounted at the base of a metal coupling block (MCB) which holds the laser and couples it thermally to the TE. The unbalance signal from the thermistor bridge is amplified and applied to a pass transistor which finds itself in one of two possible states: off or full on. Thus the TE is run with a form of off-on circuit and is continuously cycled between these two states. The advantage of this circuit is that the transistor is driven to a high conducting state and therefore has a minimum voltage drop and least sensitivity to temperature fluctuations. In order to succeed in this design, it was necessary to match the TE to the transistor in order to obtain a joint drop of 5 V. The current into the TE has a fixed amplitude of about 1 A, and the power supply should have a rating of at least 1.5 A.

Besides the laser, the MCB also contains a load resistor whose purpose is to supply a small amount of heat (1/8 W). This heat drives

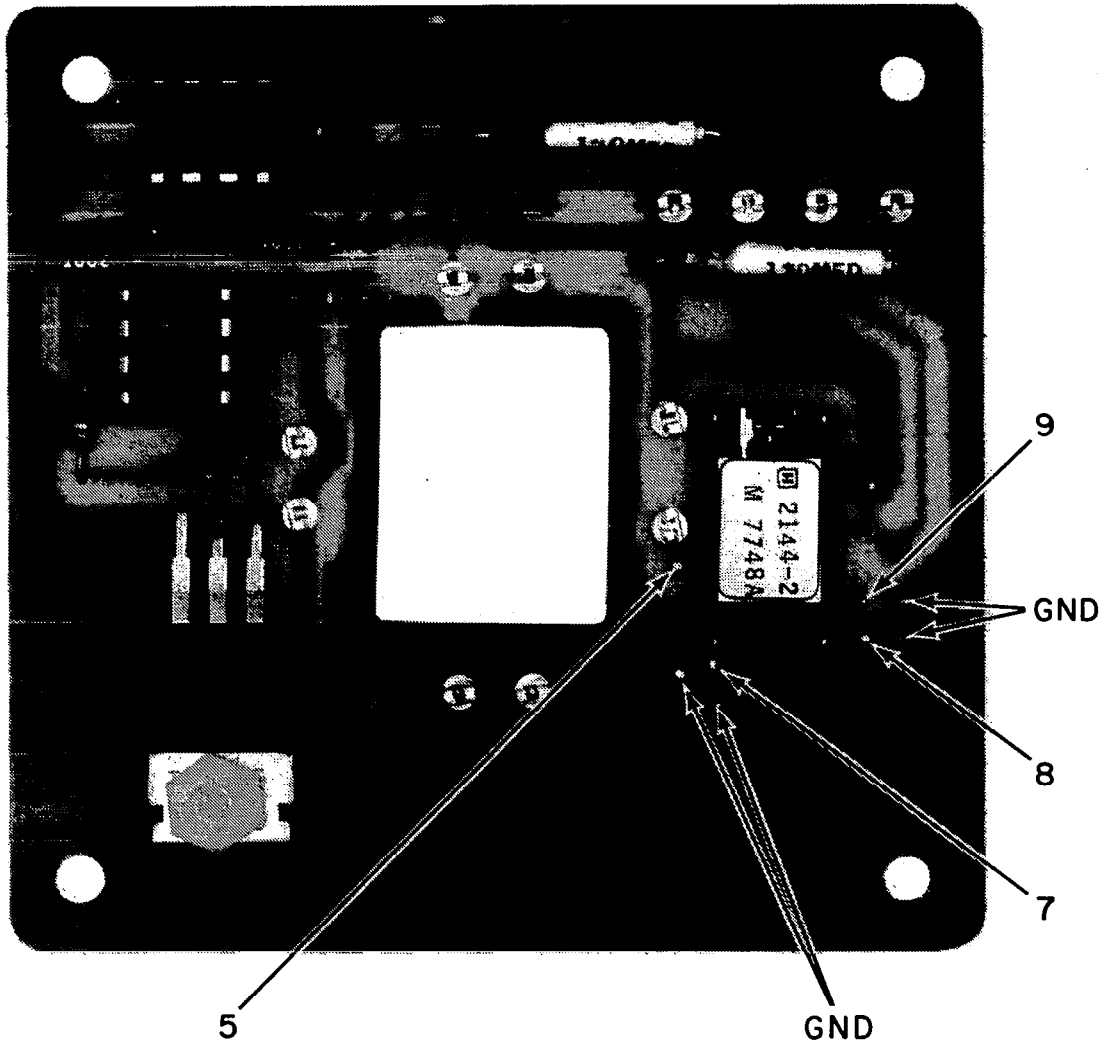
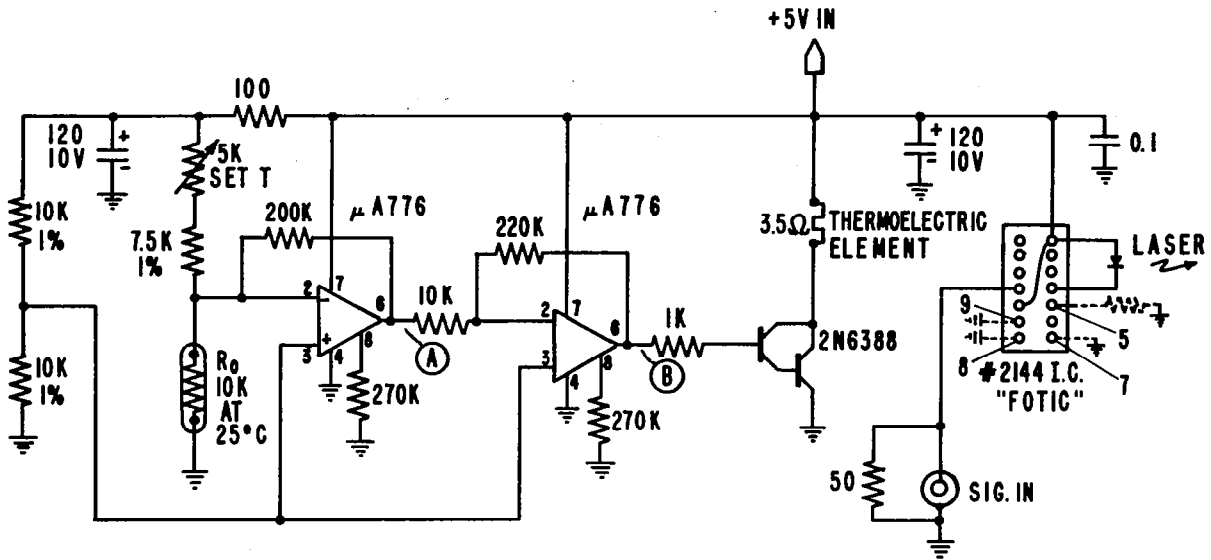
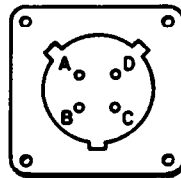


Figure 2. Photograph of the PC board showing parts layout.

the laser to a temperature above ambient, thus exercising the TE even below ambient temperature. Good temperature control around ambient is therefore easier to obtain. Without this heater, only temperatures



CONDITION	(A)	(B)
"FLIP"	+2.57	+3.75
"FLOP"	+2.37	+0.48



- A N.C.
- B
- C +5V
- D GND

Figure 3. Temperature control circuit.

above ambient could be stabilized, although self-heating from the laser also serves to raise the uncooled operating temperature. An additional advantage of the heater is that it reduces the time the laser operates at temperatures below the set point, such as might occur in early morning start-up. The optimum value for the heat put in by this load resistor has not been established, and might very likely turn out to be higher than that used. The circuit gain is adjusted to provide control within  $\pm 0.1^\circ\text{C}$ . However, enough gain is available so that the temperature limits can be reduced by a factor of 10, or more, if desired. A photograph of the assembled circuit is shown in Fig. 4(a).

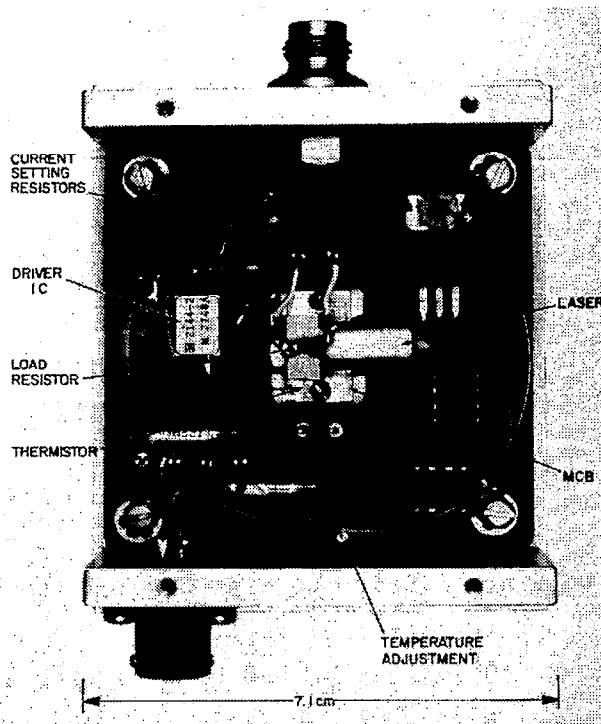


Figure 4(a). Photograph of interior of complete unit.

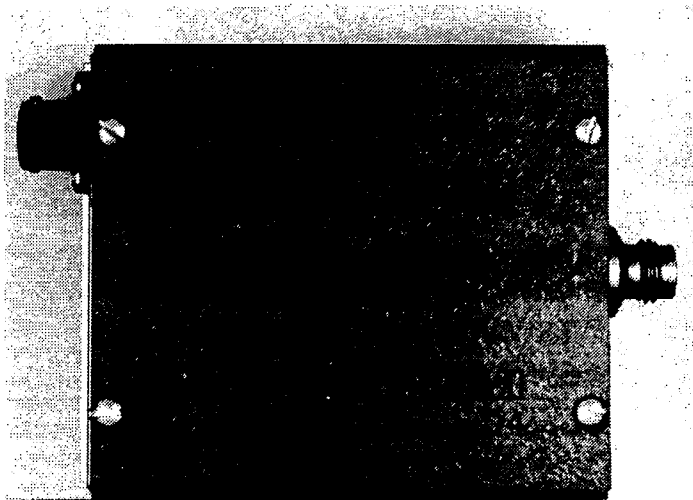


Figure 4(b). Exterior of complete unit.



## 2. Laser Driver

The current to the laser is delivered by an IC developed for the Government and supplied to us by NASA. It accepts input TTL pulses and delivers current pulses to the laser of up to 150-mA amplitude. The unit seems to perform very well, although there are two areas in which it could be improved. First, the current setting is awkward since external resistors have to be used for intervals finer than 25 mA, and second, the bias is fixed at 50  $\mu$ A, which is often below the desirable threshold bias of 50 to 100 mA.

An exterior view of the complete module is shown in Fig. 4(b). For convenience we provide a summary of the procedure used to adjust the laser driving current. (Refer to Fig. 5 for a schematic diagram of the IC and to Fig. 2 for terminal locations.)

Any current up to 150 mA can be had by selecting a resistor whose value is given by  $R = 1.83/I$ , where R is in ohms and I in amperes, and soldering it between terminal 5 and ground. Otherwise, various discrete current values can be obtained by selecting one or more of the terminals marked 7, 8, and 9 and connecting them to ground. This selects one of several possible resistance values and yields a current given by the above equation.

## C. THEORETICAL DISCUSSION

The injection laser is sensitive to temperature, which affects all its properties. The wavelength of a laser depends on the energy band-gap of the material and on the cavity which selects the particular modes. If, in the course of operation, there is an alteration in these properties, for example, if the contacts age, permanent changes in the current flow can occur which affect the mode gain or the average temperature. This may result in a permanent change in the emission wavelength. In general, however, it is possible to eliminate these

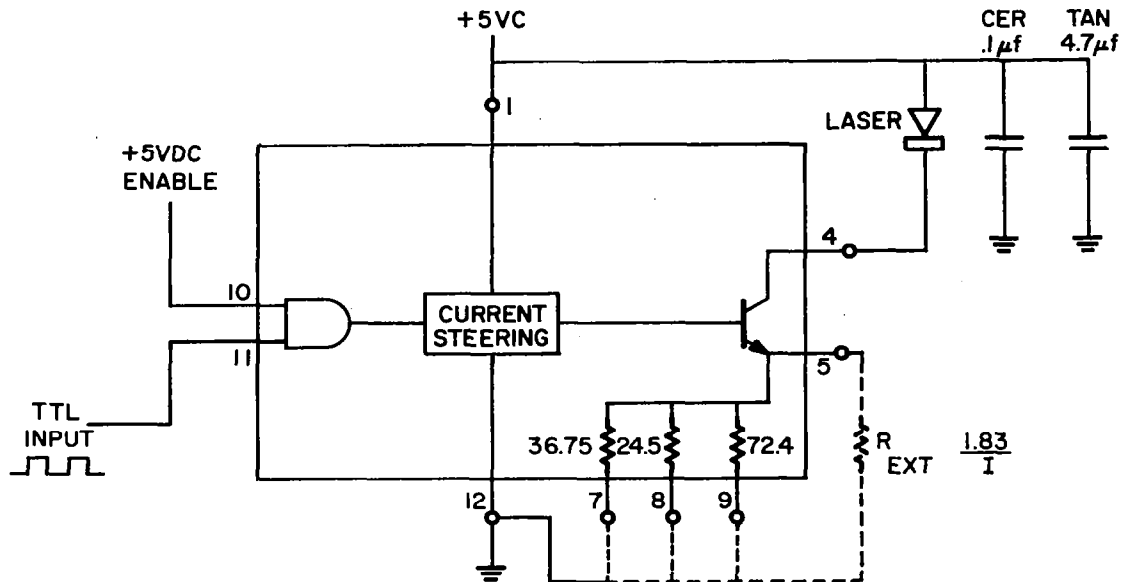


Figure 5. Driver IC functional diagram.

factors by proper laser design on the one hand, and by aging (burn-in) on the other. In the discussion to follow we will be concerned with properly designed and/or aged lasers in which this effect can be neglected.

As is well known, the threshold current of a laser can be characterized by an exponential dependence on temperature of the form  $I_{th} = I_0 \exp(T/T_0)$  where  $T_0$  is typically  $100^\circ\text{C}$  to  $120^\circ\text{C}$  for AlGaAs devices. This threshold sensitivity manifests itself in a large change in output as the temperature is changed (to be discussed below).

A change in output power, however, does not necessarily result in a wavelength change because most well-made single-mode lasers maintain their wavelength over a substantial range of outputs. Thus, it is not so much the change in output power but the change in temperature and wavelength itself which is our main concern.

As mentioned before, a change in bandgap affects the energy released in recombination. A common expression for the dependence of bandgap on temperature is [1]

$$E_g(T) = 1.52 - 5.8 \times 10^{-4} T^2 / (T + 300) \quad (1)$$

from which we obtain for the change of energy with temperature

$$\frac{dE_g}{dT} \sim -5.8 \times 10^{-4} \left[ 1 - \left( \frac{300}{T + 300} \right)^2 \right] \sim 0.435 \text{ meV}/^\circ\text{C} \quad (2)$$

This is the change observed for the spontaneous emission, the laser emission being not quite the same because of other factors such as the density of states dependence on temperature and band filling. For an 8200-Å laser, the bandgap-induced change is about 2.5 to 3 Å/°C. The spontaneous emission line is very broad (200 Å) so that many Fabry-Perot modes can arrange themselves within it, and a slight shift in this spontaneous envelope does not necessarily shift the emission line. Because of this and other effects, such as the gain suppression by the oscillating field [2], the bandgap has to change by a minimum amount before the wavelength abruptly jumps to a new value. As a rough guide, we may assume the wavelength will change when the spontaneous emission shifts by an amount equal to one or two Fabry-Perot mode spacings, i.e., 5 to 10 Å for most of our lasers. Thus the shift may occur for changes in temperature of 2 to 4°C.

Superimposed on this discontinuous shift is a smooth change in wavelength due to a change in cavity length, induced by the thermal

1. M. B. Panish and H. C. Casey, Jr., J. Appl. Phys. 40, 163 (1969).
2. M. Yamada and Y. Suematsu, IEEE J. Quantum Electron. QE-15, 743 (1979).

expansion of the material and the change in refractive index. These effects are conveniently described by [3,4]

$$\frac{d\lambda}{dT} = \lambda \left[ \frac{1}{L} \frac{dL}{dT} + \frac{1}{n} \frac{dn}{dT} \right] \quad (3)$$

Since  $1/L \, dL/dT \sim 0.6 \times 10^{-5}/^{\circ}\text{C}$  and  $1/n \, dn/dT \sim 1 \times 10^{-4}/^{\circ}\text{C}$ , the index change is the dominant effect, and the wavelength shift is given by

$$\frac{d\lambda}{dT} \sim 0.82 \text{ \AA}/^{\circ}\text{C} \quad (4)$$

As far as external disturbances are concerned, such as changes in ambient temperature, the problem is relatively straightforward. The laser is mounted on a TE, and with suitable sensors and control circuits its temperature can be kept constant within any desired limits. Much more important is the self-heating effect. The power output of a laser is given by

$$P_o = I V \eta \quad (5)$$

where  $I$  is the current,  $V$  the applied voltage, and  $\eta$  the light emission efficiency of the laser. For typical lasers,  $\eta \sim 0.06$  to  $0.20$ , so that most of the input power appears as heat. The largest fraction of this power dissipation occurs in the laser cavity due to nonradiative recombination. Significant amounts are also released in the contacts, and in the bulk material by photon absorption. This heat raises the cavity temperature, beginning at the instant current is applied to the laser. Thus it is clear that no matter how we cool the laser, its temperature will begin to rise as soon as a pulse is applied. If the

3. M. Cardona, Int. Conf. Semicond. Phys., Prague, 1960, p. 388.
4. S. I. Novikova, Sov. Phys. Solid State 3, 129 (1961).

pulse is very short, 100 ns or less, the rise will be very small, and if we bias the laser to threshold, the steady current will develop an average temperature in the laser, which will change by a much smaller amount as the driving pulse is applied, because junction impedance is now low, or what amounts to the same thing, the laser differential emission efficiency is high, on the order of 50%. If pulses starting from zero bias are used, it is definitely advantageous to use a pulse scheme such as Manchester coding, where the duty cycle is relatively constant, as that will stabilize the average temperature.

The conclusions to be drawn from the above discussion are the following:

- (a) Keeping a constant current flowing through the laser and varying the temperature, we expect a gradual shift in wavelength, and after a 2 to 4°C change, a jump by a few Å to a new wavelength.
- (b) Keeping the temperature constant and varying the dc current, we expect similar behavior due to self-heating.
- (c) Keeping the TE temperature constant and increasing the pulse duty cycle, we expect the laser cavity temperature to shift; the amount of shift and corresponding mode jumps depend on the particulars of heat flow out of the laser.

In the next section we describe experimental results on a CDH laser, and we show that the wavelength shift, even with standard pulse-code modulation, can be less than 10 Å, our design goal.

## D. EXPERIMENTAL RESULTS

### 1. Temperature-Induced Wavelength Changes

The laser used for these tests was a CDH type with single-spectral line emission over a broad current and output power range. This laser

also had a single-spot near-field output with no discernible beam structure, and thus was typical of a good single-mode laser.

- (a) The laser was driven with 100-ns pulses having an amplitude of 90 mA. The duty cycle was 0.01%. The laser was held on a TE and the heat-sink controlled at various temperatures while the spectrum was recorded. The results of the experiments are shown in Fig. 6. The stepwise increase in wavelength and the gradual shift are clearly seen. From this curve one obtains a value of  $\sim 0.75 \text{ \AA}/^\circ\text{C}$  for the gradual, index-induced change in wavelength. To be sure, the slope from which this measurement is taken is somewhat different at different temperatures. The abrupt jump is about  $5 \text{ \AA}$  which is one longitudinal mode step for this laser. It is to be noticed that the change from one step to the next occurs in about  $2^\circ\text{C}$ . All of these results are in good agreement with the discussion given in section C.
- (b) The same laser, on the TE, was driven with a steady dc current of 91 mA. Here the results were similar although the position of the step was different. In the range of  $16$  to  $21^\circ\text{C}$  there was no step (see Fig. 6) indicating that there exists a region in which the laser is more stable against mode shifts. In this case the total change was  $3 \text{ \AA}$  over a temperature change of  $5^\circ\text{C}$ . Clearly this is a more desirable operating region for dc operation. In general, whether pulsed or not, one may expect that certain regions of operating temperature will provide a more stable wavelength in regard to mode jumps, and it is important to be able to set the laser at that temperature. A potentiometer on the TE power supply provides such an adjustment.
- (c) The laser was kept at a heat-sink temperature of  $22.5^\circ\text{C}$  while the pulse length was kept constant at 150 ns. The duty cycle

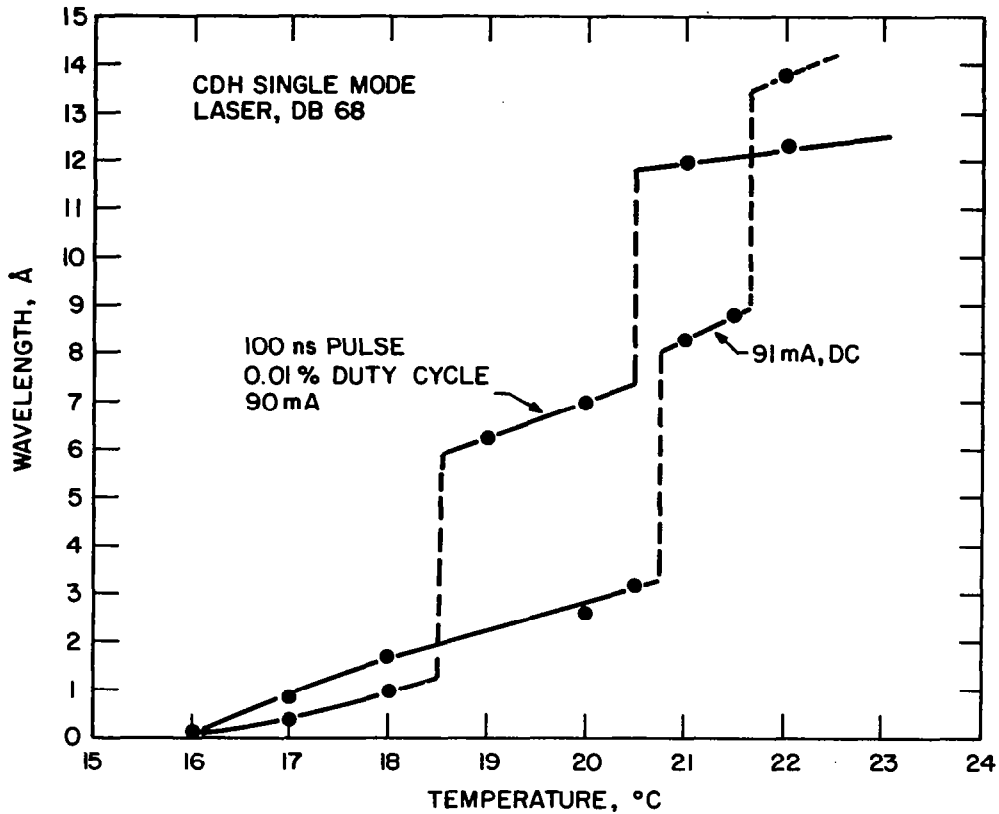


Figure 6. Wavelength shift vs temperature.

was varied from 1.5% where we assume no heating, to dc where we have the maximum heating.

The results are given in Table 2 and shown in Fig. 7.

TABLE 2. EXPERIMENTAL RESULTS

<u>T (°C)</u>	<u>Duty Cycle (%)</u>	<u>Current (mA)</u>	<u>Wavelength (Å)</u>
22.5	1.5	77	8476
22.5	15	77	8478
22.5	100	77	8482.4

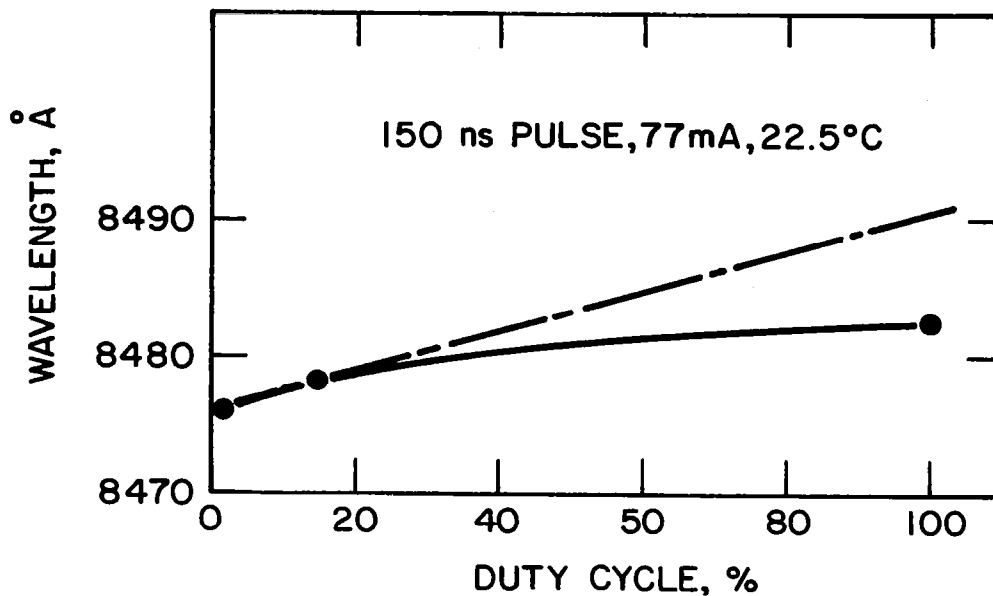


Figure 7. Wavelength dependence on duty cycle, CDH laser.

From this we obtain  $0.083 \text{ \AA/mA}$  for the gradual wavelength change with current where we assumed no further wavelength reduction in going from 1.5% to 0% duty cycle. Combining this with the previously established value for the temperature-induced wavelength change of  $0.75 \text{ \AA/}^\circ\text{C}$  we obtain  $0.11^\circ\text{C/mA}$  for the temperature change caused by internal heating. These figures are important for the present application because they show the maximum allowed current change for a given temperature and wavelength change. However, we also see that changing the duty cycle from essentially zero to 100% does not have to cause a mode jump even though the current-induced temperature change is large enough to produce mode jumping under some conditions. At some other operating temperature this stability may not occur, as shown in Fig. 6. The dashed line in Fig. 7 shows that the duty cycle dependence is far from linear. This departure is due to the fact that at low duty cycles the diode temperature rises linearly because the temperature depends



on adiabatic heating of a given volume of material, whereas at longer duty cycles, the temperature depends on the mechanism of heat flow out of the diode. The wavelength change as the duty cycle is changed simulates the conditions in a pulse-modulation scheme where the information is coded as a variable pulse repetition rate. The total wavelength change with maximum measured duty cycle change is  $6.4 \text{ \AA}$  which is below the required  $10\text{-}\text{\AA}$  maximum excursion. Even though the above data show that it is possible to operate the laser under these conditions, it seems more desirable to use a constant-input-power method such as Manchester coding. It may be mentioned that another method has been proposed to stabilize the wavelength [5], namely, one which supplies a current to the TE cooler whose magnitude is proportional to the current driving the laser. However, it seems that such a method succeeds only if the TE response time is fast enough to follow the temperature fluctuations, which does not seem to be an easy requirement.

The present measurements can be used to obtain a value for the thermal resistance  $R_{th}$  for this laser.  $R_{th}$  is defined as the temperature increase resulting from a power input of 1 W expressed in  $^{\circ}\text{C}/\text{W}$ . As we have seen, the temperature rise per unit current is  $0.11^{\circ}\text{C}/\text{mA}$ , and for an applied bias of 1.7 V we obtain

$$\frac{0.11^{\circ}\text{C}}{1.7 \times 10^{-3}} = 64^{\circ}\text{C}/\text{W}$$

Lasers with lower values of  $R_{th}$  would show smaller wavelength changes as the current or duty cycle are changed.

---

5. M. Yamada, F. Iida, S. Kido, and R. Ishibashi, Trans. ICE Japan E61, 896 (1978).

## 2. Output Fluctuations Due to Temperature Cycling

It was observed that the output from the fiber end fluctuated with time even when the laser was driven with a dc signal. In order to elucidate the origin of this fluctuation, we performed several experiments. The current through the TE was displayed on an oscilloscope together with the signal picked up from the end of the fiber, using a fast optical detector. As shown in Fig. 8, the optical detector showed spikes synchronized with the TE driving pulses. These are, however, low in amplitude and are as fast as the current pulse. Thus it seems likely that they represent an electrical interaction in the circuit, such as a drop in the driver output due to the insufficient capacity in the 5-V supply or inadequate wiring. More precise data were obtained by measuring the output of the fiber with a calibrated detector-dc amplifier system. We also recorded the temperature of the MCB using a sensitive thermocouple. In Fig. 9, curve c shows that the temperature excursions of the MCB due to the cycling of the pass transistor are  $0.018^{\circ}\text{C}$  peak to peak.

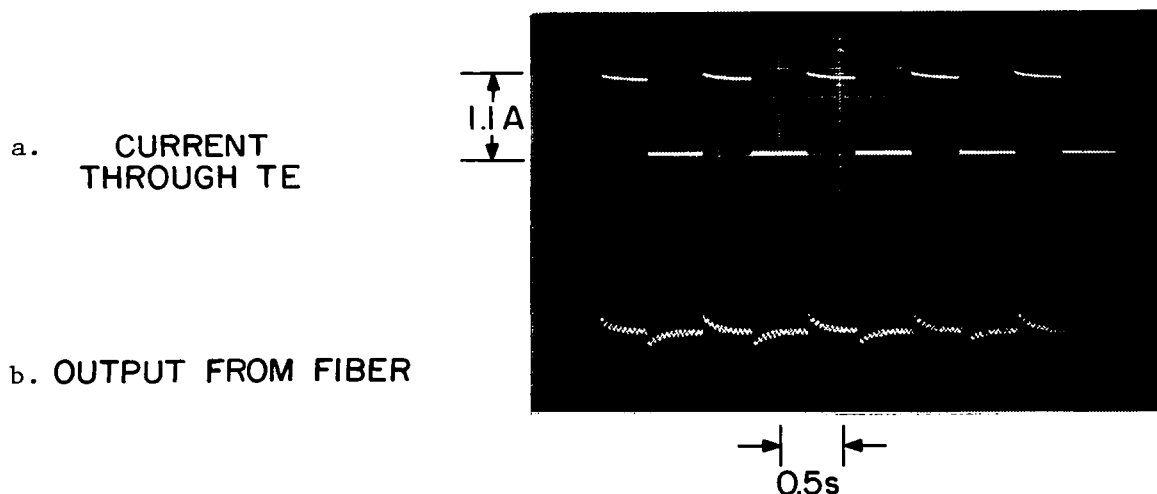


Figure 8. Output spikes due to TE pulsing.

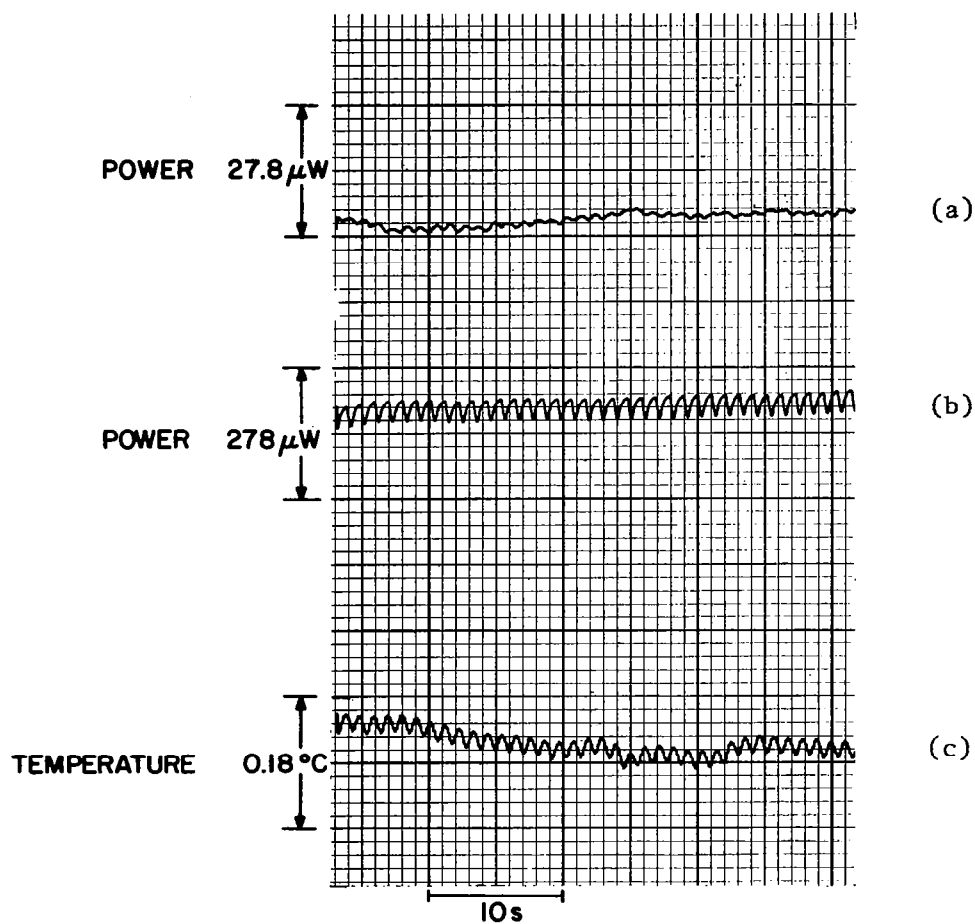


Figure 9. Comparison of fiber output with temperature of the MCB. (a) Laser driven with separate power supply, (b) laser driven with internal IC, and (c) temperature of MCB.

Figure 9(b) shows the output from the fiber, and Fig. 9(a) the same output when the driving IC was bypassed and the laser operated from an external dc source. It can be seen that the periodicity in all three traces is the same, and thus attributable to the temperature cycling. That the fluctuation in Fig. 9(b) is due to electrical pickup is confirmed by the fact that it is eliminated when a separate power supply is used. The cycling visible in Fig. 9(a) is due to the

temperature-induced changes in threshold current. This can be seen by referring to Fig. 10 which shows the output for this particular laser measured at the fiber, for two different temperatures. From Fig. 10 it is established that a  $1^{\circ}\text{C}$  change in temperature causes a  $\sim 200\text{-}\mu\text{W}$  change in output.

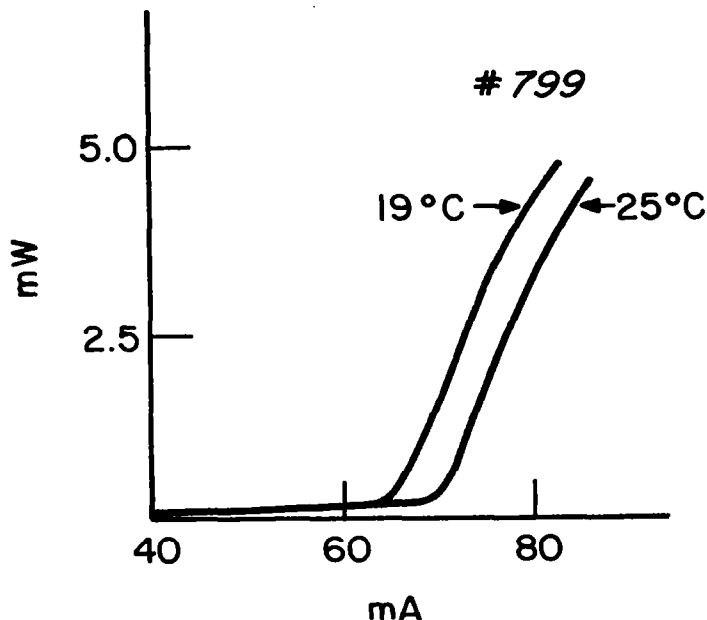


Figure 10. Laser output (measured at fiber end) for 19 and 25°C.

For the measured peak-to-peak temperature excursion shown in Fig. 9(c) of  $0.018^{\circ}\text{C}$  we thus deduce an output change of  $3.6\ \mu\text{W}$ . The output change actually measured, as shown in Fig. 9(a), is  $1.5$  to  $2\ \mu\text{W}$  peak-to-peak; the discrepancy we believe to be due to the fact that the temperature shown in Fig. 9(a) was measured near the TE, and these pulsations are smoothed out at the laser position, some distance away from the TE.

The slower random fluctuations seen in Fig. 9 are probably caused by drift in the unstabilized dc amplifiers used in these experiments. The fluctuations shown in Fig. 9(a) amount to 0.05% of the peak output of 3.89 mW measured in this case. An electrical interaction between the two parts of the circuit, the driver and the TE supply, can be eliminated by making sure the wiring is adequate, by using a power supply of sufficient capacity, or by electrically decoupling the two circuits.\* The temperature control circuit is therefore considered to be satisfactory for the present application.

### 3. Optical Feedback Effects

It has been known for some time that reflection of radiation back into the laser leads to various undesirable effects [6,7]. In particular, the wavelength of the laser is affected by this feedback and there can be changes in modal properties. Other effects noted are the occurrence of spontaneous oscillations, threshold changes, noise, and instability, but we are mainly concerned with the effect feedback has on wavelength. An example of such a situation is shown in Fig. 11 where we see spectra taken from the laser measured directly (without fiber) and after coupling to various fibers provided with hemispherical or flattened ends. Figure 11(a) shows the spectrum obtained when no fiber was used, Fig. 11(b), when the laser was coupled to a fiber having the end rounded very slightly, as shown in the photomicrograph. In this case, reflection from the fiber end is sufficient to disturb

---

\*NASA Langley has advised us that they have solved this problem by using remote sensing to control the power supply voltage.

6. I. Ikushima and M. Maeda, IEEE J. Quant. Electron. QE-14, 331 (1978).
7. R. Lang and K. Kobayashi, IEEE J. Quant. Electron. QE-16, 347 (1980).

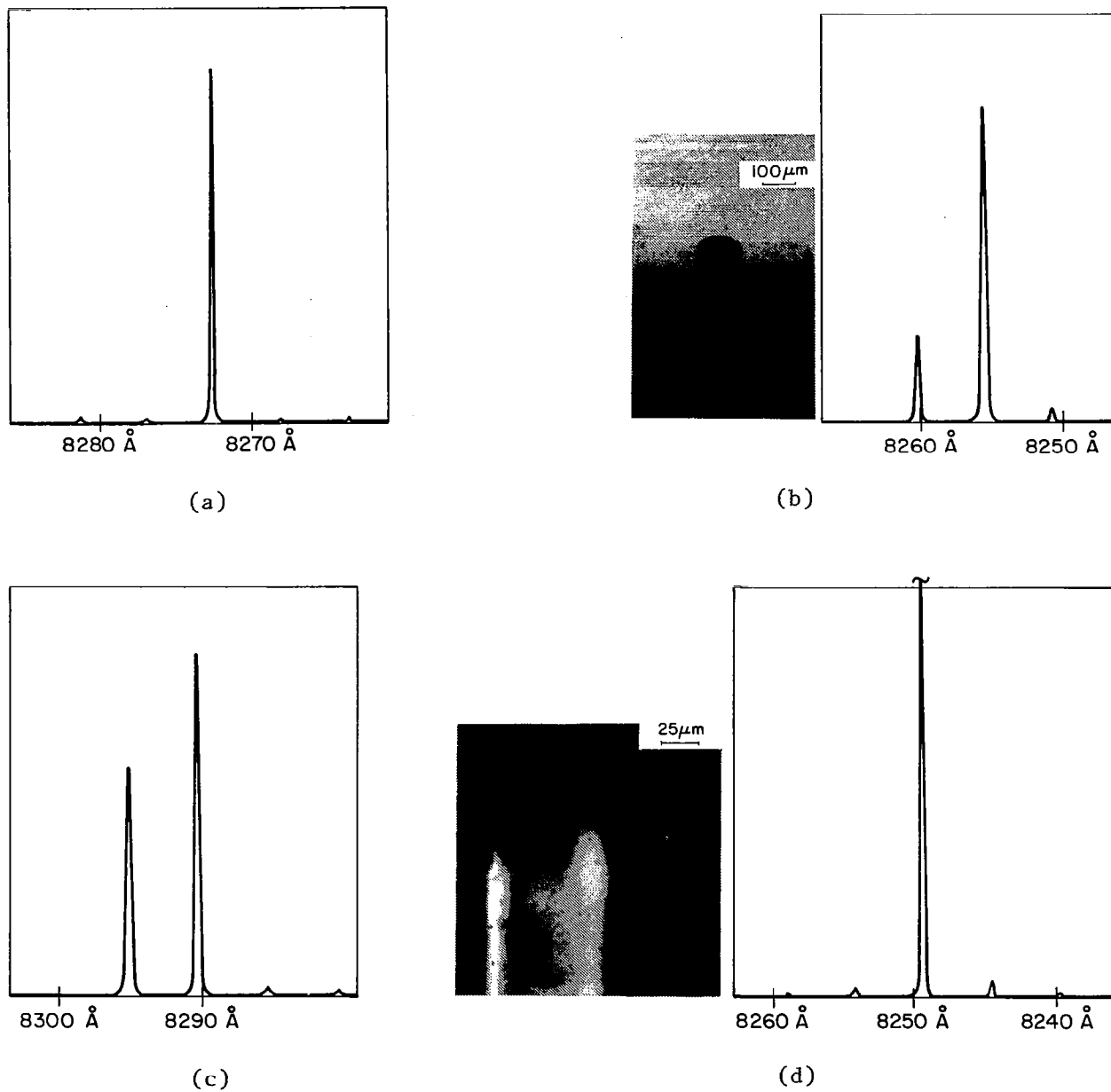


Figure 11. Optical feedback effects: (a) is output from laser before coupling; (b) after coupling to graded index fiber having the input end beaded as in photomicrograph; (c) same as (b) except that the end of the fiber (away from laser) was immersed in high index fluid; (d) output from fiber with more rounded input end.

the mode structure. When the fiber was removed, the direct output spectrum (not shown) reproduced that of Fig. 11(a). However, changing the reflection from the far end of the fiber pigtail by immersing it into a high-index liquid also produced a change [Fig. 11(c)], which indicates that undesirable feedback occurs from both the front and the back end of the fiber. Using a different, more rounded fiber end [Fig. 11(d)] again produced a single-mode spectrum, although at a different wavelength. These results suggest that coupling to a well-rounded fiber end can result in a single-line spectrum if the laser is initially capable of it, but that there is some optical feedback involved, from either the front or the back surface of the fiber, that affects the exact wavelength delivered. It seems likely that for best performance, a nonreciprocal element may have to be included in the optical path. The beneficial effect of the rounded hemispherical fiber end (beyond the increased coupling efficiency) is probably due to the reduced back reflection from the divergent optical system formed by the front surface of the lens.

## II. COUPLING OF SINGLE-MODE LASERS TO THIN-FILM OPTICAL WAVEGUIDES

### A. INTRODUCTION

The initial objective of this part of the program was to develop a method of coupling one of the longitudinal modes of a multimode junction laser to a diffused optical waveguide while not coupling or only weakly coupling the other longitudinal modes.

Because of the inherent sensitivity of gratings to wavelength we investigated the properties of grating couplers to thin-film optical waveguides. This work is described in subsection B, below.

We found that grating couplers do indeed have the property of coupling one wavelength more strongly than another and this property could be enhanced by increasing the coupling length. The strength of the coupling, however, depends inversely on the coupling length through undesired random scattering. Thus, while it was found possible to suppress an undesired axial mode spaced  $6 \text{ \AA}$  from a desired mode by more than 20 dB, the overall coupling efficiency was less than 1%. Although improvement of the gratings to give higher coupling without sacrificing selectivity appears possible, a more practical alternative presented itself in that, as described in subsection B below, relatively high-power, single-longitudinal-mode junction lasers are now available which make mode selection unnecessary.

Under these conditions it seemed advantageous to look at non-wavelength selective but more efficient coupling methods than the grating coupler. We thus decided to study prism couplers which are well understood and promised to provide compact and efficient couplers for transferring the single-longitudinal-mode of advanced junction lasers to optical waveguides. This work in turn was divided into two parts.



The first part is described in subsection C, below. Here we describe the development of a miniature cylindrical lens system which enables us to make a compact junction laser thin-film optical waveguide coupler. The lens system mounts directly on the laser and is small enough to be encapsulated with the laser in a header or other miniature protective seal. The lens system is designed to produce a symmetric beam which may, as a matter of choice, be either converging or diverging. At the same time, a large fraction of the laser light (greater than 90%) is collected.

The experimental system described in subsection C brings the laser beam to a symmetrical focus with a beam waist of about 100  $\mu\text{m}$  approximately 1 cm from the laser. The beam waist is chosen to be suitable for prism coupling to the optical thin-film waveguides used in this program.

We think that the miniature cylindrical lens system described here will find many applications in conjunction with the use of junction lasers in fiber optics, thin-film optical waveguides, and data processing and storage systems such as optical disc recording systems.

The actual coupling of the laser light to  $\text{LiNb}_x\text{Ta}_{1-x}\text{O}_3$  (LNT) on  $\text{LiTaO}_3$  waveguides and the construction of a small unit combining the laser cylindrical lens assembly with the prism-optical waveguide assembly which was delivered to NASA is described in subsection D. Single-wavelength power of over 0.5 mW in the optical waveguide was readily obtained. The coupling efficiency is approximately 10%. Much higher efficiencies are expected for future systems based on this approach. The demonstration reported here used less than optimum cylindrical lenses and mechanical arrangements to meet the time constraints of this program.

We expect that optimized arrangements could demonstrate powers on the order of 2 mW in the waveguide. These arrangements do not require

any new technology or mechanisms, and the theory and art described in this report appear adequate to reach this latter value.

## B. SELECTIVE GRATING COUPLING

Grating coupling to thin-film optical waveguides has been extensively described in the literature. We will briefly review the coupling conditions and then describe how the grating coupler may be used to preferentially couple a single wavelength mode from a group of axial laser modes.

A schematic diagram of a thin-film waveguide and grating for coupling is shown in Fig. 12. We consider that a parallel beam of light of wavelength  $\lambda_o$  impinges on the grating at an angle to the waveguide normal of  $\theta$ . In a focused beam the beam waist associated with the focused beam spot may be considered parallel for this purpose. The waveguide mode to be excited has an effective index  $n_e$ . A phase grating is produced as an embossment in the waveguide as shown or, more commonly, as an added transparent corrugated layer placed on the waveguide surface. The grating period is  $d$ . In either case it is assumed that the grating does not appreciably perturb the waveguide properties. Under these assumptions the condition for coupling between the input beam and the waveguide is

$$\sin \theta_o = n_e - \lambda_o/d \quad (6)$$

The intensity of light coupled will depend on the grating strength and the interaction length  $L$ . It must be noted that, as in the prism coupler described below, the grating couples light out of the waveguide as well as into the waveguide so that the grating must be terminated at some point within the input beam waist ( $W_T$ ). A complete discussion of this matter is given by Tamir [8].

8. T. Tamir, "Beam and Waveguide Couplers," in Integrated Optics, 2nd ed., T. Tamir, Ed. (Springer-Verlag, NY, 1979) pp. 90-93.

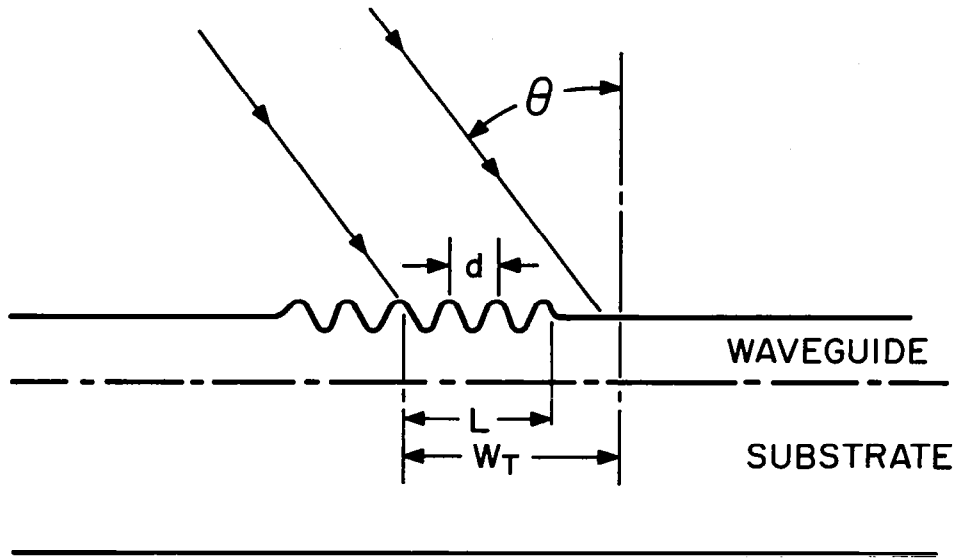


Figure 12. Thin-film waveguide and corrugated grating coupler. The amplitude of the grating is exaggerated.

If at the wavelength  $\lambda_0$  the angle  $\theta_0$  exactly satisfies Eq. (6), at some other value of wavelength  $\lambda$  Eq. (6) will be exactly satisfied at a different angle ( $\theta$ ). It has been shown that at a fixed wavelength the intensity coupled will vary with angle as

$$\frac{I}{I_0} = \left[ \frac{\sin \left( \frac{2\pi L \Delta\theta}{2d} \right)}{\frac{2\pi L \Delta\theta}{2d}} \right]^2 \quad (7)$$

where  $\Delta\theta = |\theta_0 - \theta|$

and  $I_0$  is the intensity coupled at  $\theta_0$  which exactly satisfied Eq. (6).

If  $\theta$  remains constant and  $\lambda$  is varied, we have

$$\Delta\theta = - \frac{1}{\cos \theta} \frac{\Delta\lambda}{d}$$

giving

$$\frac{I}{I_0} = \left[ \frac{\sin \left( \frac{\Pi L \Delta\lambda}{d^2 \cos \theta} \right)}{\frac{\Pi L \Delta\lambda}{d^2 \cos \theta}} \right]^2 \quad (8a)$$

where

$$\Delta\lambda = \lambda - \lambda_0$$

This may be written in a normalized form as

$$\frac{I}{I_0} = \left[ \frac{\sin \left( \frac{\Pi (L/\lambda_0) (\Delta\lambda/\lambda_0)}{(d/\lambda_0)^2 \cos \theta} \right)}{\frac{\Pi (L/\lambda_0) (\Delta\lambda/\lambda_0)}{(d/\lambda_0)^2 \cos \theta}} \right]^2 \quad (8b)$$

Equation (8) can be used to determine the coupling length required to reduce the coupling for an undesired axial mode at  $\lambda$  spaced from a desired mode at  $\lambda_0$  by  $\Delta\lambda = \lambda_0 - \lambda$ . The argument in Eq. (8)  $[\Pi (L/\lambda_0) (\Delta\lambda/\lambda_0)] / [(d/\lambda_0)^2 \cos \theta]$  may be written as

$$A_1 (L/\lambda_0) (\Delta\lambda/\lambda_0) \quad (9)$$

where  $A_1 = \Pi / (d/\lambda_0)^2 \cos \theta$

Generally  $A_1$  will be on the order of 10. Using  $A_1 (L/\lambda_0)$  as a parameter, we have plotted  $10 \text{ Log } (I/I_0)$  or  $I/I_0$  in dB as a function of  $\Delta\lambda/\lambda_0$  in Fig. 13. The dashed lines are the complete expression given by Eq. (8b) for a value of  $A_1 (L/\lambda_0) = 10^4$ . The solid lines connect the loss minima of Eq. (8b) and thus serve as boundaries for the lowest discrimination that will be obtained for given values of  $A_1 (L/\lambda_0)$ .

The selectivity of the coupler depends on the coupling length. This is analogous to the use of gratings in spectrographic applications

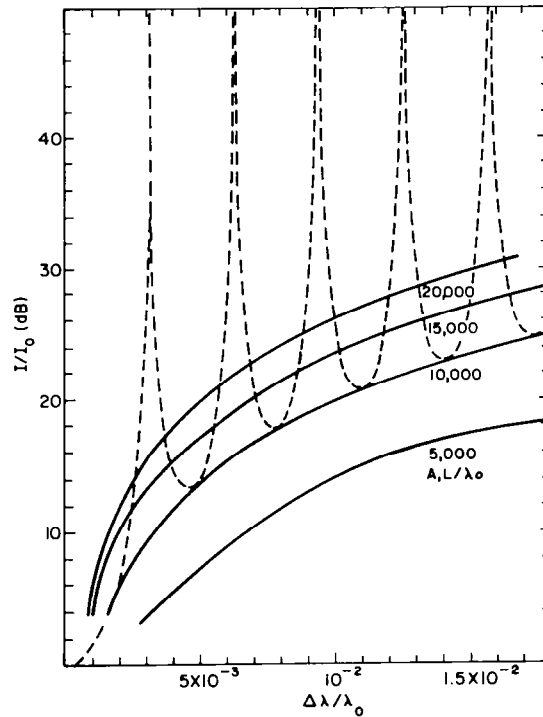


Figure 13. Selectivity of waveguide grating coupler. The grating space and angle are chosen to optimize the coupling at  $\lambda_0$ .  $I_0$  is the intensity coupled at  $\lambda_0$ .  $I$  the intensity coupled at some other wavelength  $\lambda$ .

where the resolution of the spectrograph is proportional to the grating aperture. In the coupler application it is desirable to have a large coupling length to suppress undesired modes. On the other hand, efficient coupling makes other demands on the coupling length. In theory efficient coupling would be independent of the coupling strength, requiring only that the coupling length be properly chosen to match the coupling strength. In practice, however, gratings with weak coupling strength requiring long coupling lengths suffer from the effect of imperfections much more severely than strong gratings requiring short coupling lengths. Thus, the actual requirement of high selectivity imposes limitations on the actual coupling percentage that will be practically available.

## Experiment

### Optical Waveguide and Grating Preparation

We used a  $\text{LiNb}_x\text{Ta}_{1-x}\text{O}_3$  on  $\text{LiTaO}_3$  (LNT) optical waveguide produced prior to the start of this program. These guides are described by Hammer and Phillips [9,10]. The particular waveguide (LNT35155) was formed on a Y plate of  $\text{LiTaO}_3$  that was pretreated with  $\text{Li}_2\text{CO}_3$ . We deposited 800 Å of Nb on this plate and it was diffused at 1183°C for 2½ hours in an  $\text{O}_2$  atmosphere. The resulting guide had a single TE and a single TM mode. The effective guide index ( $n_e$ ) was approximately 2.18.

The grating was formed by depositing a stripe of Shipley\* AZ-1350 photoresist ½ mm wide by 5 mm long. The long dimension was perpendicular to the "C" crystallographic axis. The photoresist was exposed in a holographic setup and developed to produce a grating with grating vector parallel to the "C" axis and grating space (d) of 0.66 μm giving a predicted coupling angle of 65° (measured  $\theta = 66^\circ$ ).

### Junction Laser Preparation

RCA Laboratories AlGaAs laser sample 541-992 was fitted with two fibers mounted at right angles to each other in an attempt to obtain a symmetric beam. See subsection C for a complete description of the symmetrizing of junction laser beams using cylindrical rods as lenses. The work described in this subsection was done before the development described in subsection B. Here a 50-μm (0.002-in.) fiber was mounted close to and parallel to the junction plane and a second fiber of 380-μm diameter (0.015-in.) was placed in contact with the first fiber and at

---

9. J. M. Hammer and W. Phillips, Appl. Phys. Lett. 24, 545 (1974).

10. W. Phillips and J. M. Hammer, J. Electronic Materials 4, 549 (1975).

\*Shipley G. Inc., Newton, MA.

right angles to the junction plane. Both fibers were cemented in place with epoxy. The emerging beam was not quite symmetric but was a great improvement over the raw laser beam in angular symmetry. The diverging angle was approximately 3 degrees. A 20-cm focal length conventional lens was then used to focus the light on the grating. The distances were chosen so that the beam waist focused on the grating was approximately 1 mm ( $10^3 \mu\text{m}$ ) in diameter. All the light coupled into the waveguide by the grating was extracted approximately 2 mm downstream from the grating edge by a prism film output coupler. The measured coupling efficiency was 0.6%.

Light directly from the laser and light that had been coupled into the waveguide via the grating and then prism coupled out of the waveguide was examined spectrographically. The resulting spectrographic traces are shown in Fig. 14. The results of careful measurements of the amplitudes are given in Table 3. The intensity of the 8472-Å line which is spaced 6 Å from the 8478-Å line is reduced by the coupler such that  $I_{(8472)}/I_{(8478)} = 1.45/0.012$  or a factor of 121. This corresponds to -20.8 dB.

TABLE 3. MEASUREMENT RESULTS

<u>Wavelength (Å)</u>	<u>Relative Intensity</u>	
	<u>Directly from Laser</u>	<u>Through Grating Coupler and Waveguide</u>
8478	1.00	1.00
8472	1.45	0.012
8447	0.88	<0.001
8421	0.43	<0.001
8415	0.13	<0.001

Other lines of relative intensity below 0.001 are not listed.

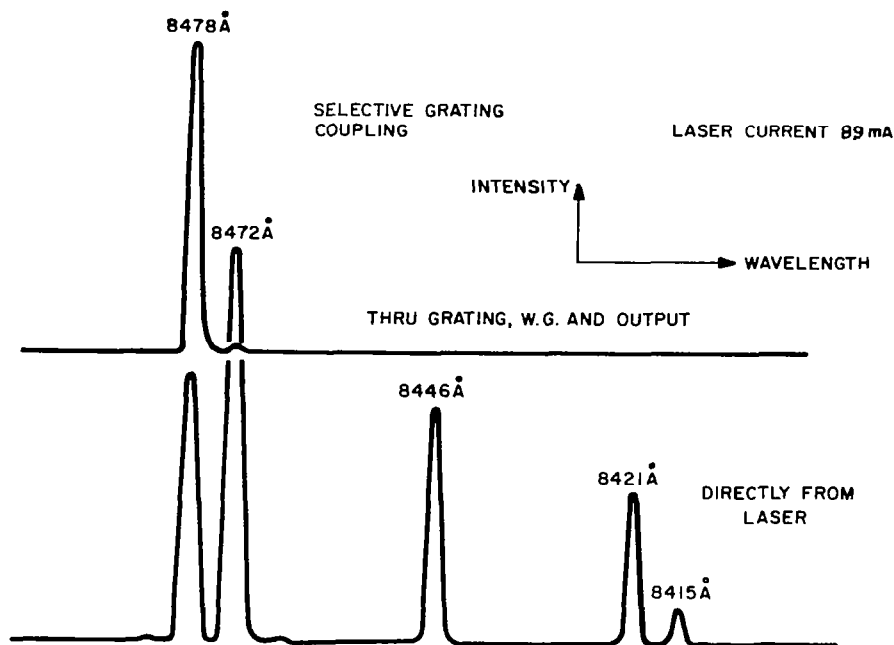


Figure 14. Traces of the spectral output. Lower trace: directly from the junction laser; upper trace: light grating coupling into LNT waveguide and prism coupled out of waveguide.

We may compare this with the theoretical expected results using Fig. 13. For our coupling angle and grating space the factor  $A_1$  is calculated to be 12.85. With a 1-mm spot ( $L = 1 \text{ mm}$ )  $A_1 L/\lambda = 15,297$ . Thus the curve for  $A_1 L/\lambda = 15,000$  will be approximately correct. For a 6-Å spacing between lines we have  $\Delta\lambda/\lambda = 0.00071$ . With these values we would expect  $I_{8472}/I_{8478}$  to be -20 dB or less which is in good agreement with our observations. As expected, the other (further spaced) lines are reduced below detection sensitivity.

We note again the difficulty of having an interaction length as great as 1,000  $\mu\text{m}$  and still maintaining efficient coupling. The observed 0.6% coupling efficiency might be improved by better grating preparation. A very smooth grating with nearly perfect grating shape



would be required for any significant improvement in coupling efficiency without sacrificing resolution. With the availability of single-mode lasers it seemed more fruitful to combine a single-mode laser with other non-selective but more efficient coupling methods.

### C. MINIATURE CYLINDRICAL LENS SYSTEM FOR COLLECTING, SYMMETRIZING, AND FOCUSING JUNCTION LASER BEAMS

#### 1. Introduction

In many applications of junction lasers, it would be desirable to render the highly divergent and axially asymmetric laser beam into a more tractable form. At the same time, whatever the application, it is necessary to use relatively high numerical aperture optics to collect all the laser light. Angular beam divergences at right angles to the laser junction plane of approximately  $40^\circ$  are common. In nonfiber coupling applications high numerical aperture microscope objectives or similar lenses have been used to collect all the light. When the application requires a symmetric beam, correcting cylindrical optics are used after the collecting lens. This arrangement frequently requires very long total optical path lengths ( $\sim 1$  meter), creating very bulky systems.

In this subsection a relatively simple collecting and symmetrizing cylinder lens system will be described. In this system, illustrated in a general form in Fig. 15, two small cylinders of refractive indexes and diameters chosen on the basis of the theory below are set with axes perpendicular to each other. The cylinder nearest the laser is arranged with its axis parallel to the junction plane. The cylinders collect the laser light and result in an emerging beam which retains a "square" cross section as it propagates away from the lens system. In many applications the lenses can be chosen so that no further optical elements are required - i.e., prism or grating coupling to planar or

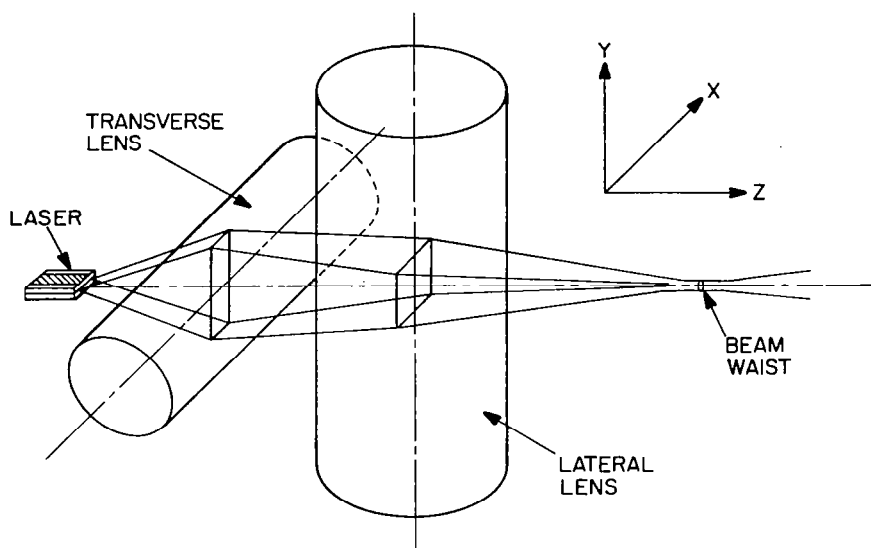


Figure 15. Perspective illustration of cylinder lens system for symmetrizing junction laser output.

stripe optical waveguides. (See subsection D.) The lenses are located sufficiently close to the laser and are of sufficiently small size that the laser and the lenses may be considered a unit that might readily be encapsulated or hermetically sealed.

## 2. Theory

The calculation of the required lens diameters, refractive indexes, and positions is relatively straightforward. In Fig. 16 the rays at the half-power angles in both transverse and lateral direction and the lens cross sections are superimposed in one plane so that the required trajectories become apparent. For this figure we imagine the lateral direction rotated around the Z axis of Fig. 15 by  $90^\circ$ . In Fig. 16, the rays and lens cross section shown by solid lines lie in the Y-Z

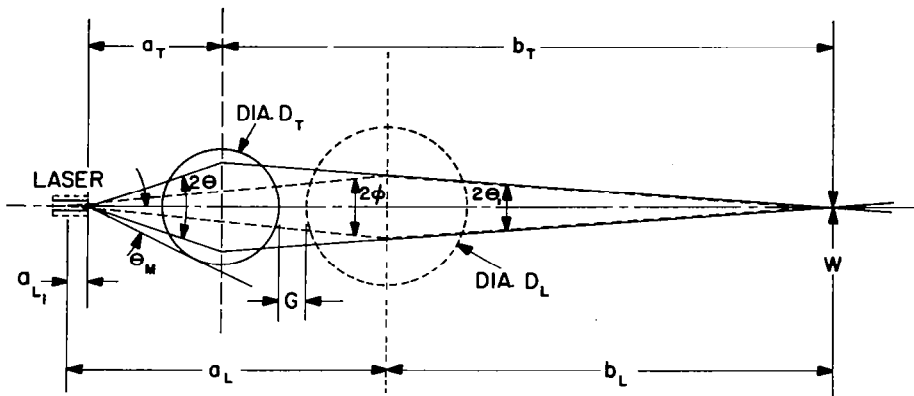


Figure 16. Ray diagram for calculating cylinder lens parameters to symmetrize junction laser output. The lateral direction is shown by dashed lines and has been rotated  $90^\circ$  around the Z axis.

plane and are referred to as Transverse quantities using the subscript T. This Y-Z plane is perpendicular to the junction plane of the laser. The rays and lens cross section shown using dashed lines lie in the X-Z plane which is parallel to the junction plane and are referred to as Lateral quantities using the subscript L.

We consider the case where both lenses are right circular cylinders.  $2\theta$  is the transverse angular spread of the laser measured at the half-power point;  $2\phi$  is the lateral angular spread of the laser similarly measured.  $2\theta_1$  is the desired angle of convergence after the lens system. Clearly, to meet requirements of symmetrizing the beam,  $\theta_1$  must be the same in both the lateral and transverse planes.

We assume that in the transverse direction the beam originates from a point source located at the laser facet. The point is actually the intersection of a line parallel to the X axis (in the junction plane) and the Y-Z plane. The length of this line is the width of the lateral laser mode ( $l_L$ ) at the laser facet. The width of the transverse mode ( $\sim 1.0 \mu\text{m}$ ) can be ignored with negligible error in this lens

calculation. In the lateral plane we assume the beam originates at a point source a distance  $a_{L_1} \leq \ell_L/2 \tan \phi$  behind the laser facet.  $a_{L_1}$  depends, in fact, on the character of the beam waist at the laser facet. For some lasers  $a_{L_1} \sim 0$ . For a complete circular cylinder the principal plane degenerates to a single plane through the cylindrical axis.  $a_T$ ,  $(a_L - a_{L_1})$  are the physical distances of the transverse and lateral lens axes from the light sources.  $b_T$ ,  $b_L$  are the respective distances to the beam waist  $W$ .  $W$  is required to be equal in both the transverse and lateral directions. Because of the presence of the transverse lens in the object space of the lateral lens,  $a_L$  is less than the optical length of the lateral object distance. Similarly, the presence of the lateral lens in the image space of the transverse lens makes  $b_T$  less than the optical length of the transverse image distance.

We compensate for this in the subsequent calculation by increasing the lateral object distance by the first order correction  $(n_T-1) D_T$  and the transverse image distance by  $(n_L-1)D_L$ . Here, and in the remaining calculation,  $n_T$  is the refractive index of the transverse lens and  $n_L$  that of the lateral lens.

The focal length of a circular cylinder of refractive index  $n$  and diameter  $D$  is  $f = (4 (n-1)^2/n)D$  [11]. Thus,

$$\begin{aligned} f_T &= \left[ 4 (n_T-1)^2/n_T \right] D_T \\ f_L &= \left[ 4 (n_L-1)^2/n_L \right] D_L \end{aligned} \tag{10}$$

11. M. Born and E. Wolf, Principle of Optics, 2nd Ed. (Macmillan, NY, 1964) p. 161.

The lens formulas can be written as follows:

$$\frac{1}{a_L + af_T} + \frac{1}{b_L} = \frac{1}{f_L} \quad (11)$$

$$\frac{1}{a_T} + \frac{1}{b_T + bf_L} = \frac{1}{f_T} \quad (12)$$

To ensure that  $\theta_1$  and  $W$  are equal for both planes requires that

$$\frac{(a_L + af_T) \tan \phi}{b_L} = \frac{a_T \tan \theta}{b_T + bf_L} \quad (13)$$

The value of  $\theta_1$  is given by

$$\tan \theta_1 = \frac{a_T}{b_T + bf_L} \tan \theta \quad (14)$$

Here the appropriate optical path lengths are corrected for computational convenience in the form  $af_T$  and  $bf_L$  where

$$a = \frac{4 (n_T - 1)^3}{n_T} \quad (15)$$

$$b = \frac{4 (n_L - 1)^3}{n_L}$$

These are the first order corrections mentioned earlier. Finally, to ensure that the beam waist lies at a common point along the Z axis for both the lateral and transverse plane, it is necessary that the physical distance of the beam waist from the laser facet be the same in both planes. Thus,

$$a_T + b_T = a_L - a_{L_1} + b_L \quad (16)$$

We know  $\theta$ ,  $\phi$ , and  $a_{L1}$  and we choose  $\theta_1$  or  $W$  which are not independent.

We also choose  $n_T$ ,  $n_L$  and  $D_T$  or  $f_t$  which leaves the five unknowns;  $D_L$  related to  $f_L$  through Eq. (10),  $a_T$ ,  $b_T$ ,  $a_L$  and  $b_L$ . We have the five equations relating these quantities: Eqs. (11), (12), (13), (14), and (16).

In addition we have

$$\tan \theta_1 = \frac{\lambda_o}{W} \quad (17)$$

which relates the beam waist size to  $\theta_1$ . If we define a transverse lens "convergence" ratio

$$B = \frac{\tan \theta_1}{\tan \theta} = \frac{\lambda_o}{W_T \tan \theta} \quad (18)$$

and define the laser transverse to lateral divergence ratio

$$\Delta = \frac{\tan \theta}{\tan \phi} \quad (19)$$

We find the following solution

$$f_L = \frac{1}{\left[ \frac{(B\Delta + 1)^2}{B\Delta} + b \right]} \left\{ f_T \left[ \frac{(B+1)^2}{B} + a \right] + a_{L1} \right\} \quad (20)$$

$$a_T = f_T (B + 1) \quad (21)$$

$$b_T = f_T \left( \frac{1}{B} + 1 \right) - b f_L \quad (22)$$

$$a_L = f_L (B\Delta + 1) - a f_T \quad (23)$$

$$b_L = f_L \left( \frac{1}{B\Delta} + 1 \right) \quad (24)$$

We repeat Eq. (10)

$$f_T = [4(n_T - 1)^2/n_T] D_T ; f_L = [4(n_L - 1)^2/n_L] D_L$$

For the solutions of Eqs. (20) through (24) to be physically realizable, the distance  $G$  between the lens surfaces must be greater than or equal to zero.  $G$  is given by

$$G = (a_L - a_{L_1} - D_L/2) - (a_T + D_T/2) \quad (25)$$

In addition it is desirable to have both  $D_T$  and  $D_L$  large enough to accept all of the beam. The maximum angles accepted are given by

$$\theta_M = \sin^{-1} D_T/2a_T \text{ and } \phi_M = \sin^{-1} D_L/2a_L \quad (26)$$

in the transverse and lateral directions, respectively. The rejection ratios  $\theta/\theta_M$  and  $\phi/\phi_M$  should be as small as possible to ensure maximum beam acceptance, minimum cylindrical distortion and make as close an approximation as possible to the first-order length corrections. When  $\theta/\theta_M > 1$  or  $\phi/\phi_M > 1$ , all the light is not collected.

To give some appreciation of the implications of these equations we have plotted some of the results for a particular case. We assume a junction laser with a transverse beam spread of  $2\theta = 40^\circ$  and a lateral beam spread  $2\phi = 8^\circ$ . These values are high but still typical of many GaAs lasers.

Equations (17) through (26) and (10) are used as follows:  $n_L$ ,  $n_T$ , and  $D_T$  are chosen. Then for a desired beam waist  $W$  or convergence angle  $\theta$  (note from Eq. (17) that these are not independent), the required lateral lens diameter  $D_L$  and the spacings are calculated. All of the spacings and the lateral lens diameter can be determined as a fraction or multiple of the chosen transverse lens diameter. Thus, in Fig. 17, we plot the "normalized" lateral lens diameter  $D_L/D_T$  and the "normalized" spacing of the transverse lens from the laser facet  $a_T/D_T$  as a function of normalized beam waist  $W/\lambda_0$  for  $n_T$  values of 1.5, 1.6, 1.7, and 1.8. The lateral lens is assumed to have a refractive index of 1.5 (pyrex, for example). For the same

values of refractive indexes the normalized distance between the lenses  $G/D_T$  and the rejection ratio of the transverse lens  $\theta/\theta_M$  are plotted as a function of  $W/\lambda_0$  in Fig. 18. Here note that for  $n_T = 1.8$  the required distance between lenses  $G/D_T$  becomes less than zero for  $W/\lambda_0$  less than 2. Thus, it is not possible to achieve this condition. Also note that the rejection ratio is greater than one (not all the light is collected) for values of  $W/\lambda_0$  less than about 3. Thus, for the particular laser considered ( $2\theta = 40^\circ$  and  $2\phi = 8^\circ$ ) it is not possible to directly obtain spot diameters below about  $3\lambda_0$  while also collecting all the laser light using only the cylinder lens system.

What happens for very small beam waists is that if the refractive index is increased in an attempt to collect all the light, the lenses overlap. If the refractive index is decreased to avoid the overlap, the lens optical aperture is reduced below that required for full collection.

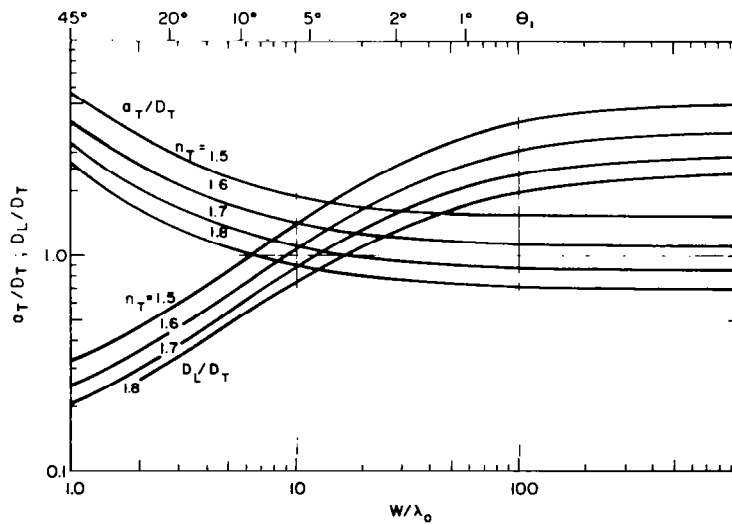


Figure 17. Plot of  $D_L/D_T$  and  $A_L/D_T$  as a function of normalized beam waist  $W/\lambda_0$ . The lens output "convergence" angle  $\theta_1$  is shown on the upper scale. The refractive index of the transverse lens  $n_T$  is the parameter.



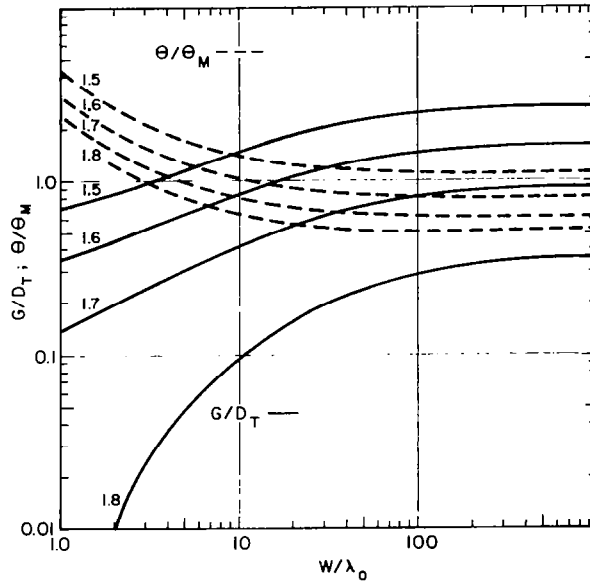


Figure 18. Plot of  $G/D_T$  and  $\theta/\theta_M$  vs  $W/\lambda_0$ ;  $n_T$  is the parameter. When  $G < 0$ , the lenses overlap. When  $\theta/\theta_M > 1$ , not all of the laser light is collected at  $n = 1.8$   $G/D_T < 0$  (negative) when  $W/\lambda_0 \sim 2.0$ .

At larger beam waists and smaller convergence angles this problem is avoided.

It should also be noted that  $\theta_1$  can be chosen to be negative (diverging symmetric beam) for some applications. Here there will be a virtual beam waist on the object side of the lenses.

The plots of Figs. 17 and 18 are included to illustrate the calculations; for any given laser the formulas presented are in closed form and the required values may be directly calculated as outlined earlier.

#### D. PRISM COUPLING TO OPTICAL WAVEGUIDES

The prism film coupler to thin-film optical waveguides has been described in great detail in a number of publications (ref. 8, pp. 86-90,

101-110). We will thus only summarize the important parameters involved in this coupling method.

Referring to Fig. 19, a laser beam is focused to have a beam waist  $W$  measured in the plane perpendicular to the waveguide. The beam waist in the plane parallel to the waveguide is less important; however, it must be considered. A large beam waist in the parallel direction raises the problem of skewness with the edge of the prism. We will thus consider that whatever the parallel beam waist dimension, it indeed is kept parallel to the waveguide plane and the prism edge. This problem is simplified for symmetric beam waists. With this caveat in mind we proceed with our description.

Restricting our attention to the beam waist perpendicular to the waveguide, we note that the beam waist center is offset from the corner formed between the prism base and perpendicular prism face by a distance  $Z$  less than  $W$ . The prism base is separated from the waveguide plane by a gap  $g$  which is less than a wavelength of light.

Light entering the prism will undergo total internal reflection from the base. The gap and angles are adjusted so that the evanescent

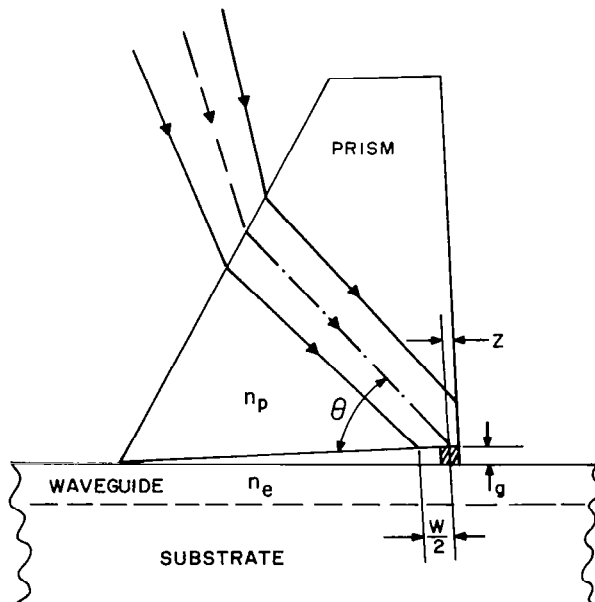


Figure 19. Schematic diagram of a waveguide-prism film coupler.

field of the totally internal reflected light in the prism and that of a waveguide mode that would be excited overlap in the gap region and have the same phase velocity parallel to the waveguide plane. Under these conditions energy will be coupled between the waveguide mode and the incident light. Initially all the light is in the prism; hence, light is lost from the prism to the waveguide mode. As the mode intensity builds up, light will be coupled from the waveguide back to the prism. The interaction must then be stopped at a point where the waveguide mode has been excited but has not yet lost too much light back to the prism. This is accomplished by having the beam waist, the gap, and the offset properly chosen (ref. 8, pp. 86-90).

The required phasematch condition is

$$n_p / \lambda_o - \cos \theta = n_e$$

$n_p$  must be greater than  $n_e$  for coupling.  $n_e$  is the effective index of the guided mode in question, and  $n_p$  is the index of the prism.

The required waist size depends on the strength of the coupling which in turn depends on the gap width. Narrow gaps produce stronger coupling coefficients and require small beam waists. The gap, in practice, is adjusted by varying the pressure used to press the prism onto the waveguide. We have found beam waists in the 50- to 200- $\mu\text{m}$  range can be accommodated with the mechanical arrangements used in our Laboratories. The correct offset  $Z$  is obtained by adjustment during alignment.

It has been shown (ref. 8, pp. 86-90) that uniform gap couplers can have maximum input coupling efficiency of approximately 80%. This value can be raised to 100% if a tapered gap coupler is used. In the output coupler, since light is continuously removed from the interaction region, 100% output coupling is achieved if the prism base is in close proximity to the waveguide for a sufficiently large distance.

An important advantage of the prism-film coupler is the fact that neither the beam waist nor the offset dimensions are critical. For

example, in a uniform gap coupler changing the beam waist from its optimum value by a factor of two only reduces the predicted maximum coupling efficiency from 80% to 70%.

We now calculate the required lens system to produce a beam waist of approximately 100  $\mu\text{m}$  for use in a prism coupler to couple light from a junction laser to a LNT waveguide. We use the formulas given in subsection C.2 above. By symmetrizing the beam we will ensure that the parallel beam waist is sufficiently small to avoid coupling problems due to skew direction. Since we had available a sapphire cylinder of 0.0965-cm diameter,  $n = n_T = 1.76$ , we made the calculation for using this cylinder as the transverse lens and a quartz cylinder with  $n = n_L = 1.4526$  as the lateral lens. Laser 732 which we used for the coupling has  $\theta = 18^\circ$  and  $\phi = 3.25^\circ$ . Using these values we obtain  $D_L = 0.189$  cm,  $a_T = 0.0754$  cm,  $b_T = 2.866$  cm,  $a_L = 0.311$  cm and  $b_L = 2.630$  cm,  $G = 0.083$  cm and  $\theta/\theta_M = 0.45$ .

#### E. EXPERIMENTAL OBSERVATIONS AND DEVICE CONSTRUCTION

A lens holder was designed similar to that shown in Fig. 20. In the original design, the groove depths are chosen to give the calculated value of the gap  $G$  between the lenses. The holder is positioned in front of the laser using a micromanipulator which provides  $x, y, z$  motion. Provision is made to allow rotation of the holder to ensure that the transverse lens is parallel to the junction. When a final lens alignment is made, as verified by measurements of the beam waist described below, the holder is cemented to the laser mount using epoxy. While the epoxy is setting, the beam waist may be monitored to allow small adjustments to compensate for any shrinkage or other motion of the epoxy.

As mentioned, the transverse lens was made from a stock sapphire rod. The rod was not accurately round, with variations on the order of

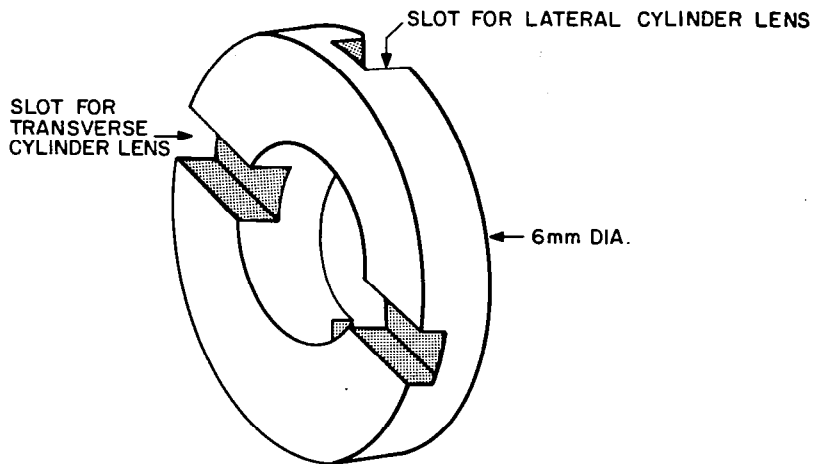


Figure 20. Sketch of an improved cylinder lens holder. The slots are spaced so that the gap is zero. Shims are used to give the desired gap and the cylinders are cemented into place.

$\pm 0.001$  cm. It was felt, however, that it would be adequate for verification of the technique. The lateral lens was fabricated by grinding and polishing a quartz rod. Because of some problems in the final polishing step, the actual lens used had a diameter of 0.193 cm rather than the 0.189 cm called for by the calculation. We expected and found that small variations of this order can be compensated for in the final lens adjustment although the final beam waist size would vary from the nominal value of 100  $\mu\text{m}$ .

The beam waist is measured using a slit detector assembly which is held on an x-y-z micromanipulator. The slit may be rotated to measure either the transverse or lateral beam waist at the same z position. The detector output is placed on the ordinate and the slit position on the abscissas of an x-y recorder plot. The minimum beam waist is found by scanning at different axial (z) positions.

Scans of the lateral and transverse beam waists obtained after the lens system is cemented into position are shown as part of Fig. 21. The beam waists are centered at a distance of approximately 2.5 cm from the

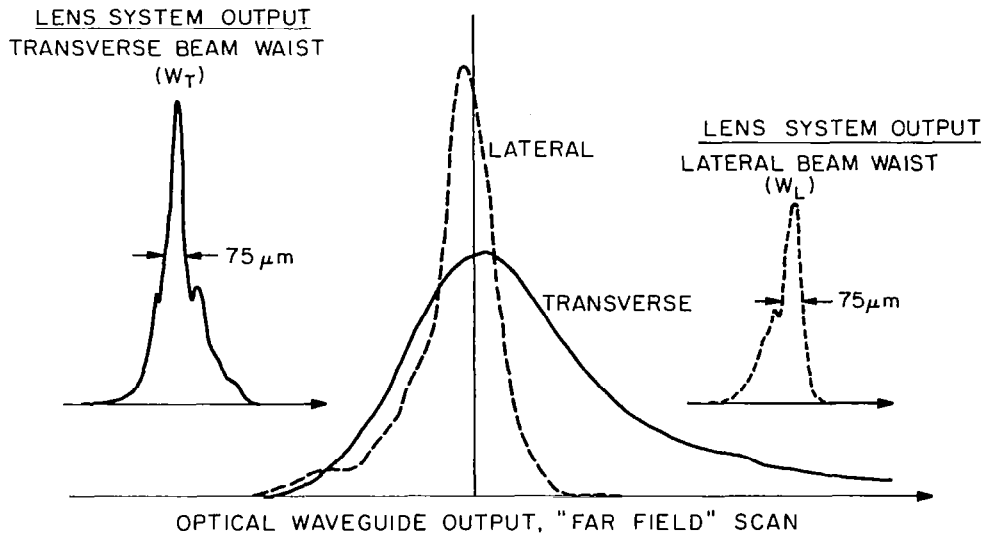


Figure 21. Experimental x-y trace of the lateral and transverse beam waist. The center figure is on x-y tracing of the far-field pattern of light coupled out of the LNT guide.

lens system. The depth of field is sufficiently long so that it is difficult to measure waist size differentials within about 0.5 cm from the waist center.

The observation of the symmetry and approximately correct beam waist size and location give reasonable agreement with the theoretical design of the miniature lens system.

The laser-lens assembly is then mounted in a compact assembly to bring the beam waist to the correct position at the coupling prism for prism coupling to an LNT waveguide. The same mount provides means of squeezing the prism in place on the LNT waveguide.

Figure 22 is a schematic diagram of the relative position of various components in the laser-lens waveguide assembly. A cross-sectional view of the mechanical details of the laser-lens waveguide mount is shown in Fig. 23. Photographs of the completed unit which

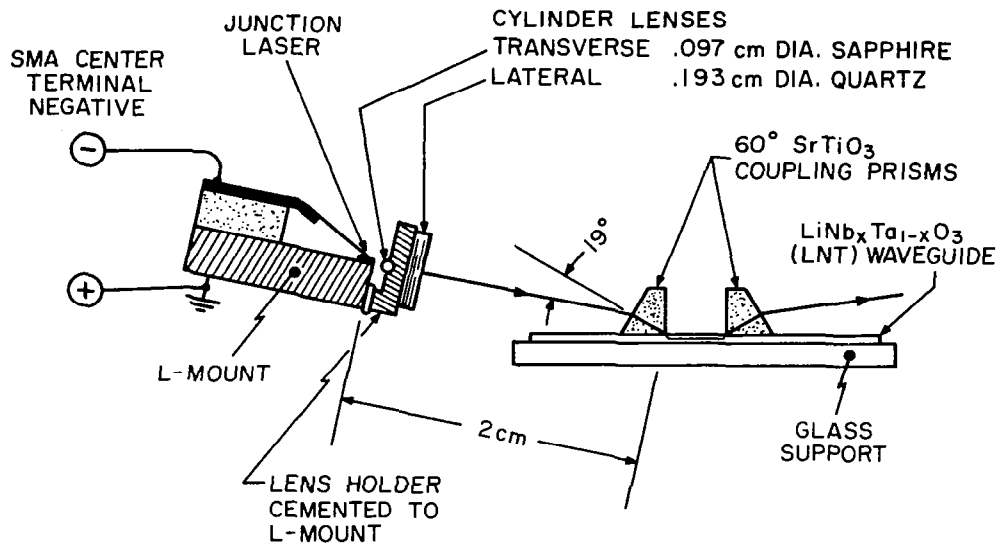


Figure 22. Schematic of laser-cylinder lens LNT waveguide assembly.

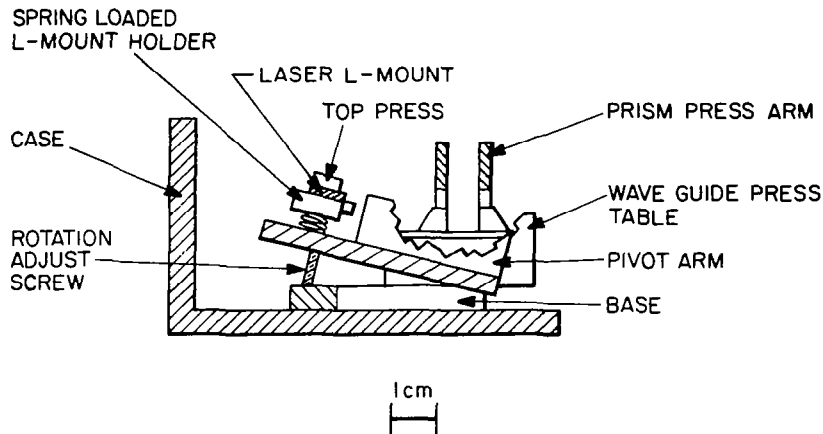


Figure 23. Cross-section of mechanical module showing details of laser-lens-LNT waveguide mount.

was shipped to NASA Langley are shown as Figs. 24 and 25. Optical power output vs laser current and the spectrum measured directly from the laser is shown in Fig. 26. The optical power and spectrum measured after the lens assembly is cemented in place are shown in Fig. 27.

Finally, the optical power output from the waveguide vs laser current and the spectrum are shown in Fig. 28. Here we are looking at the power which has been coupled into, transmitted through, and coupled out of the waveguide by the output prism coupler. The power represents a lower bound on the optical power flowing in the waveguide. The particular LNT sample has a loss of approximately 0.8 dB/cm. The interprism distance is 4 mm so that the insertion loss due to the waveguide is  $0.4 \times 0.8 \text{ dB} = 0.32 \text{ dB}$ , or a fractional transmission of 0.93. Even neglecting the waveguide loss, we see that approximately 10% of the laser light is coupled out of the waveguide in the miniature assembly. Thus a minimum of 0.5 mW of light is traveling in the waveguide at a laser current of 60 mA.

We consider this an encouraging result. The mechanical arrangement is subject to much improvement and did not allow for the fine control required to fully optimize the coupling. The lenses used were not quite optimized, and in particular the sapphire lens was not of good optical quality. The lenses were not antireflection coated, which alone causes a nonessential 20% insertion loss (at 60-mA laser current, power reduced from 4.9 mW at the laser to 3.9 mW through the lens system). There is every reason to expect that under fully optimized conditions this type of compact arrangement will yield laser waveguide coupling fractions of greater than 50%.

Finally as an illustration of the waveguide quality a far-field trace of the light coupled out of the waveguides taken with a moveable slit both parallel and normal to the waveguide plane is given in Fig. 21. The far-field trace normal to the plane shows a pattern typical of prism couplers. This has a relatively sharp rise in intensity near the prism edge. The fall-off is more gradual as more and more downstream light is removed as it passes further under the output prism.



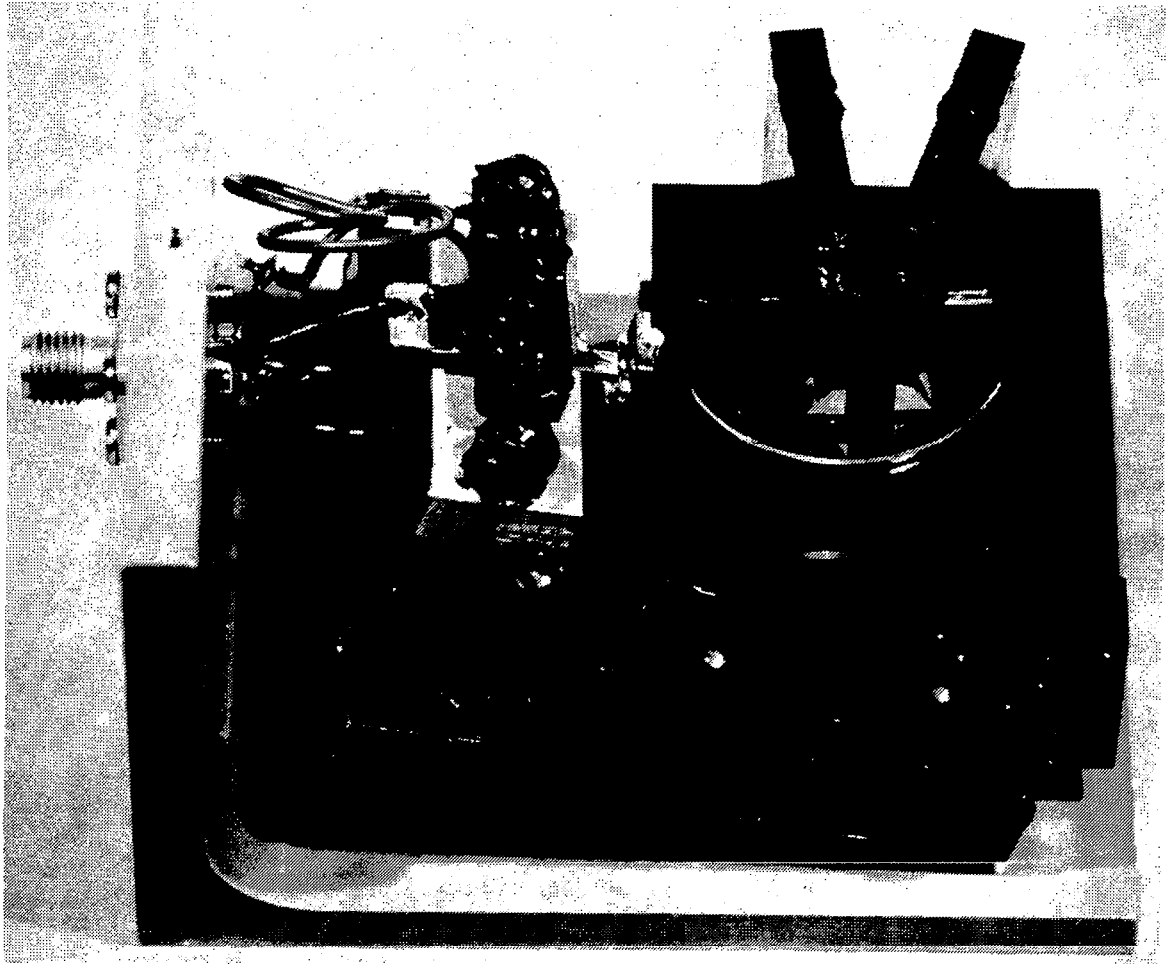


Figure 24. Photograph of final laser-lens-waveguide module.

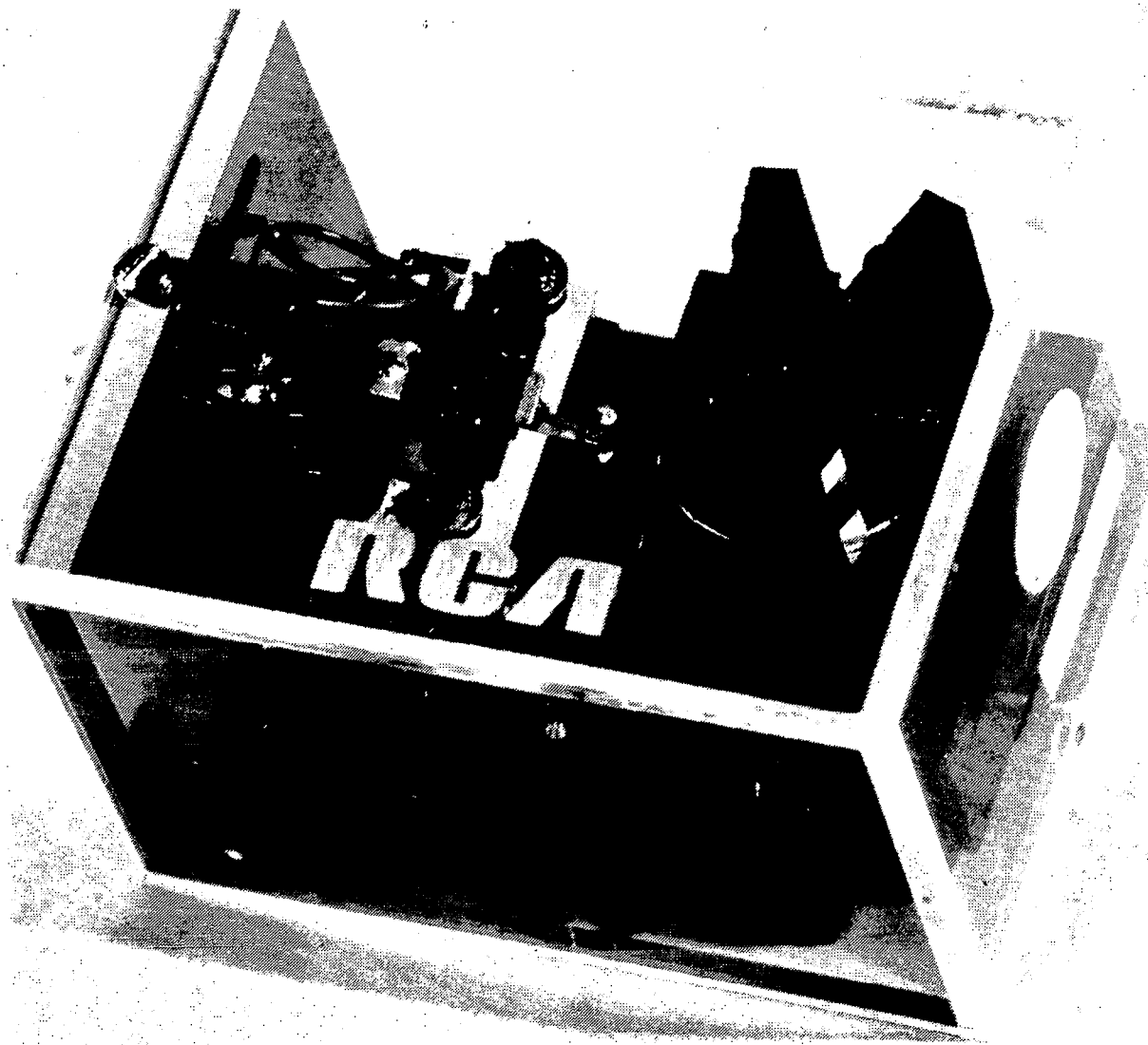


Figure 25. Photograph of laser-lens-waveguide module in protective plastic case.

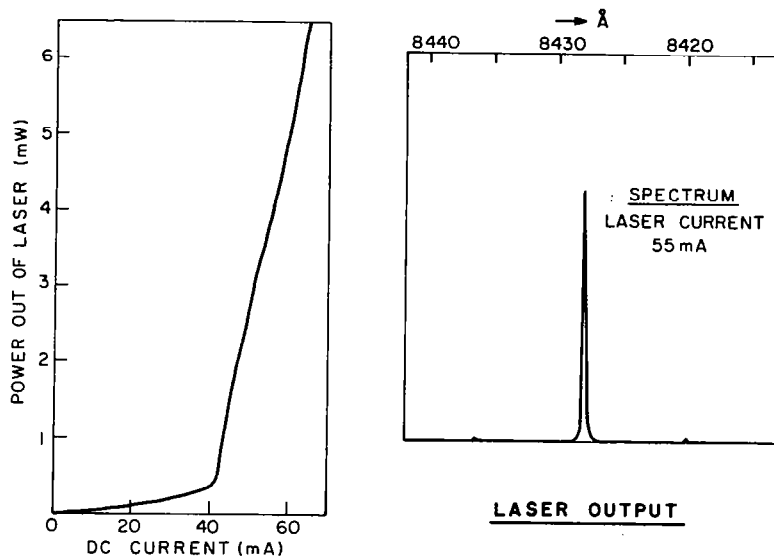


Figure 26. Plot of laser power vs laser drive current and spectrum of laser output.

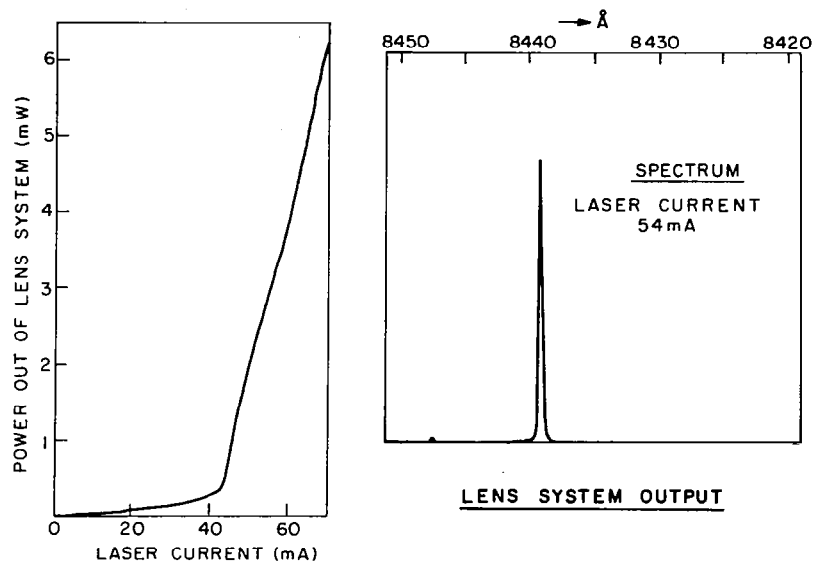


Figure 27. Plot of light intensity output of lens system vs laser drive current and spectrum of lens system output. The input is that shown in Fig. 26.

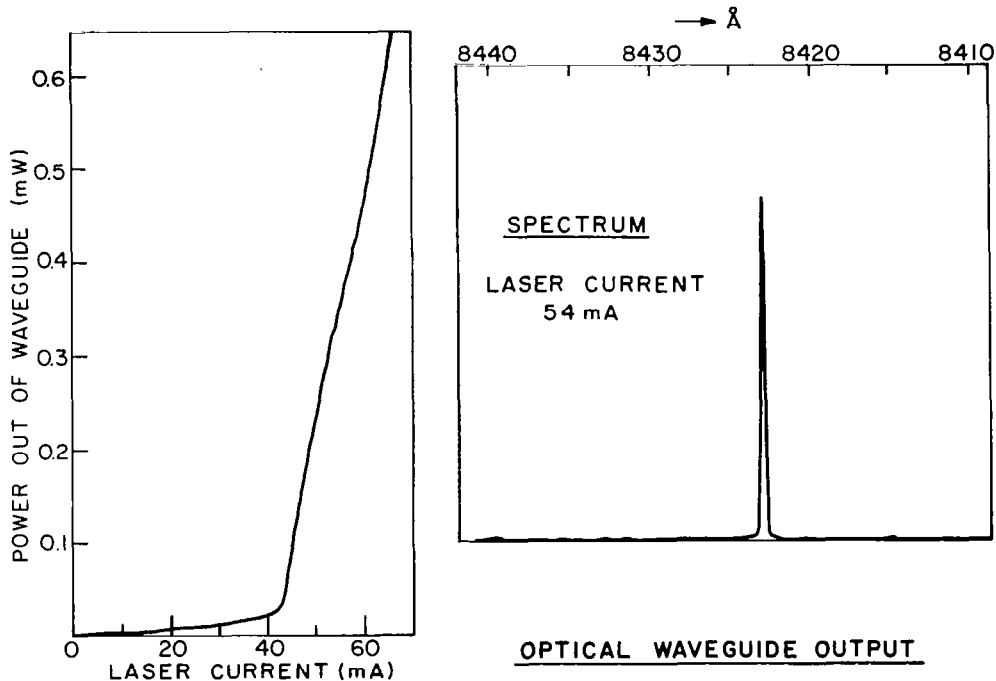


Figure 28. Plot of light intensity output coupled out of LNT guide of module vs laser current and spectrum of same. The input is that shown in Fig. 27.

Parallel to the waveguide plane the coupling traces, to a reasonable extent, the input lateral beam waist which is also shown in the drawing.

Over the range scanned the in-plane waveguide scattering is small. We estimate the in-plane scattering to be below 20 dB.

We believe these experiments demonstrate the feasibility of using compact cylinder lenses and prism couplers to construct simple, compact, and efficient couplers between junction lasers and optical waveguides. Similar lenses can be used in other applications of junction lasers which will benefit from a symmetric and low divergence optical beam.

### III. CONCLUSIONS

A temperature-stabilized laser module has been developed which is suitable for providing constant wavelength output pulses needed for optical-fiber wavelength multiplexing systems. It consists of a thermoelectrically stabilized laser, a driver, and the required power and control circuits. The module requires a single 5-V input with a rating of 1.5 A and a TTL signal input, both entering through one cable connector. The output is taken from a fiber-bulkhead connector built into the module. The wavelength stability obtainable from laser sources is discussed in general and has been measured experimentally. It is shown that for CDH lasers operating under worst-case conditions (large duty cycle changes during non-return to zero coding) the wavelength shift can be held within  $6.4 \text{ \AA}$ . In other pulse coding schemes the shift is expected to be a great deal smaller. To obtain the best performance, it appears desirable to tune the laser temperature over a few degrees in order to find a temperature region which provides the most stable spectral output. This is easily accomplished in the present thermoelectrically controlled system.

The return of part of the optical signal because of reflections at various interfaces has been found to affect the emitted wavelength. For best performance, a non-reciprocal device may have to be placed between the laser and the fiber.

Basic principles of temperature-dependent behavior of injection lasers are discussed, as they should be useful in the design of future laser modules.

In the second part of this program, coupling of a single-wavelength mode of a junction laser to in-diffused LNT ( $\text{LiNb}_x\text{Ta}_{1-x}\text{O}_3$  on  $\text{LiTaO}_3$ ) optical waveguides has been demonstrated.

Using single-mode lasers, efficient prism coupling to LNT guides was observed. A miniature and widely useful cylinder lens system

has been developed for this purpose. The lenses are sufficiently small to be incorporated with the laser in a unitized mount which may be encapsulated or hermetically sealed in standard type headers. A compact single-mode-laser-miniature-cylinder lens-LNT-waveguide-prism-coupler assembly was prepared and delivered to NASA. In this unit, which was not optimized because of time limitations, 0.5 mW of laser light was coupled into and out of the LNT guide at a laser current of only 60 mA (dc). By following the procedure described in detail in this report, it should be possible to construct miniature units of this type in which 2 mW of single wavelength junction laser light is coupled into thin-film optical waveguides.

Earlier in the program we demonstrated that grating couplers can be constructed which selectively couple one of the wavelength modes of a multimode junction laser to an LNT waveguide. To obtain the required selectivity, however, it is necessary to use a long grating where scattering due to grating imperfections makes the realization of efficient coupling difficult. To obtain both high selectivity and efficient coupling, improvements in the perfection of coupling gratings would be required.

## REFERENCES

1. M. B. Panish and H. C. Casey, Jr., J. Appl. Phys. 40, 163 (1969).
2. M. Yamada and Y. Suematsu, IEEE J. Quant. Electron. QE-15, 743 (1979).
3. M. Cardona, Int. Conf. Semicond. Phys., Prague, 1960, p. 388.
4. S. I. Novikova, Sov. Phys. Solid State 3, 129 (1961).
5. M. Yamada, F. Iida, S. Kido, and R. Ishibashi, Trans. ICE Japan E61, 896 (1978).
6. I. Ikushima and M. Maeda, IEEE J. Quant. Electron. QE-14, 331 (1978).
7. R. Lang and K. Kobayashi, IEEE J. Quant. Electron. QE-16, 347 (1980).
8. T. Tamir, "Beam and Waveguide Couplers," in Integrated Optics, 2nd ed., T. Tamir, Ed. (Springer-Verlag, NY, 1979) pp. 90-93.
9. J. M. Hammer and W. Phillips, Appl. Phys. Lett. 24, 545 (1974).
10. W. Phillips and J. M. Hammer, J. Electronic Materials 4, 549 (1975).
11. M. Born and E. Wolf, Principles of Optics, 2nd Ed. (Macmillan, NY, 1964) pp. 161.

1. Report No. NASA CR-3341		2. Government Accession No.		3. Recipient's Catalog No.	
4. Title and Subtitle SINGLE-MODE LASER STUDIES: (I) DESIGN AND PERFORMANCE OF A FIXED-WAVELENGTH SOURCE AND (II) COUPLING OF LASERS TO THIN-FILM OPTICAL WAVEGUIDES				5. Report Date October 1980	
				6. Performing Organization Code	
7. Author(s) I. Ladany and J. M. Hammer				8. Performing Organization Report No. PRRL-80-CR-13	
9. Performing Organization Name and Address RCA Laboratories Princeton, New Jersey 08540				10. Work Unit No.	
				11. Contract or Grant No. NAS1-15440	
12. Sponsoring Agency Name and Address National Aeronautics and Space Administration Washington, DC 20546				13. Type of Report and Period Covered Contractor Report (7-3-79 to 4-3-80)	
				14. Sponsoring Agency Code	
15. Supplementary Notes Langley Technical Monitor: Herbert D. Hendricks Topical Report				(Final Report No. 2)	
16. Abstract Two applications of single-mode lasers have been studied. In the first, a module was developed for the generation of a stable single wavelength to be used for a fiber-optic multiplexing scheme. The laser is driven with RZ pulses, and the temperature is stabilized thermoelectrically. The unit is capable of maintaining a fixed wavelength within about 6 Å as the pulse duty cycle is changed between 0 and 100 percent. This is considered the most severe case, and much tighter tolerances are obtainable for constant input power coding schemes. Using a CDH laser, a wavelength shift of 0.083 Å/mA is obtained due to laser self-heating by a dc driving current. The thermoelectric unit is capable of maintaining a constant laser heat-sink temperature within 0.02°C.  In the second part of the program miniature lenses and couplers have been developed which allow efficient coupling of single wavelength modes of junction lasers to thin-film optical waveguides. The design of the miniature cylinder lenses and the prism coupling techniques described will allow 2 mW of single wavelength mode junction laser light to be coupled into thin-film waveguides using compact assemblies. Selective grating couplers were also studied.					
17. Key Words (Suggested by Author(s)) Single-mode lasers Fiber-optic multiplexing scheme			18. Distribution Statement Unclassified - Unlimited  Subject Category 36		
19. Security Classif. (of this report) Unclassified		20. Security Classif. (of this page) Unclassified		21. No. of Pages 60	22. Price A04